

Article

Impact of Hard Fouling on the Ship Performance of Different Ship Forms

Andrea Farkas ¹, Nastia Degiuli ^{1,*}, Ivana Martić ¹ and Roko Dejhalla ²

¹ Faculty of Mechanical Engineering and Naval Architecture, University of Zagreb, Ivana Lučića 5, 10000 Zagreb, Croatia; andrea.farkas@fsb.hr (A.F.); ivana.martic@fsb.hr (I.M.)

² Faculty of Engineering, University of Rijeka, Vukovarska ulica 58, 51000 Rijeka, Croatia; roko.dejhalla@riteh.hr

* Correspondence: nastia.degiuli@fsb.hr; Tel.: +38-516-168-269

Received: 3 September 2020; Accepted: 24 September 2020; Published: 26 September 2020



Abstract: The successful optimization of a maintenance schedule, which represents one of the most important operational measures for the reduction of fuel consumption and greenhouse gas emission, relies on accurate prediction of the impact of cleaning on the ship performance. The impact of cleaning can be considered through the impact of biofouling on ship performance, which is defined with delivered power and propeller rotation rate. In this study, the impact of hard fouling on the ship performance is investigated for three ship types, keeping in mind that ship performance can significantly vary amongst different ship types. Computational fluid dynamics (CFD) simulations are carried out for several fouling conditions by employing the roughness function for hard fouling into the wall function of CFD solver. Firstly, the verification study is performed, and the numerical uncertainty is quantified. The validation study is performed for smooth surface condition and, thereafter, the impact of hard fouling on resistance, open water and propulsion characteristics is assessed. The differences in the impact of biofouling on the ship performance are noticed amongst different ship forms. They are mainly influenced by the portion of viscous resistance in the total resistance, relative roughness, roughness Reynolds number and advance coefficient for the self-propulsion point.

Keywords: biofouling; ship performance; container ship; oil tanker; bulk carrier; CFD

1. Introduction

Although recognized as an efficient mode of transport that has steadily enhanced safety, as well as environmental performance, over the past few decades, the maritime transport industry is transforming. Lately, in order to fulfil the new regulatory requirements and market needs, ship operators and ship owners have to improve capability of their ships to enable innovative, relevant and efficient services. Several technical and operational measures are adopted for increasing energy efficiency [1], however, it is crucial to accurately measure their effects. Namely, new regulations demand an increasing level of environmental performance, while ship operators and ship owners are faced with mounting pressure to keep up the competitiveness of their ships. As a result of this, ship operators and ship owners often hesitate to implement measure for increasing the energy efficiency due to the lack of reliable data on their effect [2,3]. The optimization of the maintenance schedule related to hull and propeller cleaning presents an important operational measure for increasing energy efficiency as ship operator or ship owner has large degree of control over it [4]. The successful optimization of maintenance schedule relies on accurate prediction of the impact of cleaning on the ship performance. The presence of biofouling on ship hull and propeller is causing an increase in roughness, which leads to an increase in ship resistance and if the ship speed is kept constant, an increase in the fuel consumption [5]. The biofouling occurrence is mostly prevented through the application of antifouling (AF) coatings, while hull and

propeller cleaning are usually performed in drydock. It should be noted that both of those measures are costly [6]. Consequently, an accurate assessment of the impact of biofouling on the ship performance is required for the proper selection of AF coatings and scheduling of hull cleaning [7].

There are different approaches for the assessment of this impact which can be classified into statistical studies, performance monitoring and approaches, based on the wall similarity hypothesis [8]. Approach based on the wall similarity hypothesis allows estimation of the fouling effect if the drag characterization of certain fouling type is performed. Drag characterization of a rough surface implies assessing the velocity decrement caused by the frictional drag of the surface as a function of the roughness Reynolds number (k^+). This velocity decrement, i.e., downward shift of the mean velocity in the log-law region of turbulent boundary layer (TBL) is called the roughness function (ΔU^+). There is no universal roughness function, however, once ΔU^+ for a certain fouling type is assessed, it can be used for the determination of frictional drag of any arbitrary body covered with that fouling type [9]. Over the last few decades, Granville similarity law scaling method has been imposed for the assessment of the impact of biofouling on the ship resistance with $\Delta U^+ = f(k^+)$ known and it has been widely used in the literature [10–14]. Nevertheless, this method has several important drawbacks, as claimed by [15]. Namely, this method can be used for the prediction of the frictional resistance coefficient of the fouled flat plate having the same length as an investigated ship, and other resistance components of fouled ship are considered to be the same as for smooth ship. What is more, this method assumes only one k^+ value and thus one ΔU^+ value over the entire flat plate. Since the k^+ value depends on friction velocity (u_τ), this assumption may lead to certain errors, as, even on a flat plate u_τ , it is not constant over the entire plate. Lastly, using Granville similarity law scaling method only increase in effective power can be estimated. As shown in [16], due to the presence of biofilm the increase in the delivered power is significantly higher than the increase in effective power.

Recently, there have been an increasing number of studies using a computational fluid dynamics (CFD) approach based on the implementation of certain ΔU^+ model within the wall function [17–20]. This approach can calculate u_τ for each discretized cell and, in that way, can obtain the distribution of u_τ values along the investigated surface. Consequently, k^+ distribution along the investigated surface will be obtained, and various ΔU^+ values will be used along the surface. Furthermore, the fouling effects on the other resistance components can be investigated, as well as the impact of biofouling on the open water and propulsion characteristics. This approach for the assessment of the impact of hull roughness on the ship's total resistance has been recently validated within [21]. Namely, within [21], it was demonstrated that CFD wall function approach can precisely determine not only the impact of roughness on the skin friction, but on the total resistance of 3D hull as well. The investigations related to the impact of barnacle and biofilm fouling on the ship propulsion performance have been presented in [8,22]. These studies demonstrated the impact of biofouling on the propulsion characteristics using CFD approach. However, both studies were performed on the example of Kreso Container Ship (KCS). Since ship resistance and propulsion characteristics can significantly vary amongst different ship forms, it would be beneficial to investigate the fouling effect on the ship performance of different ship forms.

In this study, the impact of biofouling on the ship performance of three merchant ships is analyzed. As already noted, the obtained increases due to the presence of biofouling in effective and delivered power are not equal. Therefore, it is more accurate to study the impact of biofouling on the ship performance through the analysis of the increase in delivered power and propeller rotation rate, than through analysis of the increase in effective power solely. To the best of the authors' knowledge, the impact of biofouling on the ship performance of different hull forms is investigated in this paper for the first time. This investigation is performed utilizing the CFD simulations and a Colebrook-type ΔU^+ of Grigson which is implemented within the wall function of CFD solver. Drag characterization study of hard fouling was performed by Schultz [12]. CFD model for the assessment of the impact of hard fouling on the ship resistance has been proposed in [16], where the CFD model is validated. This study can be considered as a continuation of study [16]. A verification study is carried out in order to assess grid and temporal uncertainty. A validation study for smooth surface conditions is

performed, by comparing the numerically obtained results with the extrapolated towing tank results. Finally, the detail investigation of the impact of hard fouling on the ship resistance and propulsion characteristics is performed for six different fouling conditions. The obtained results show the impact of hard fouling on the resistance and propulsion characteristics amongst different ship types, as well as on the increase in delivered power and propeller rotation rate.

2. Materials and Methods

2.1. Governing Equations

In this study Reynolds-averaged Navier–Stokes (RANS) and averaged continuity equations are used as governing equations, and they read:

$$\frac{\partial(\rho\bar{u}_i)}{\partial t} + \frac{\partial}{\partial x_j}(\rho\bar{u}_i\bar{u}_j + \overline{\rho u'_i u'_j}) = -\frac{\partial \bar{p}}{\partial x_i} + \frac{\partial \bar{\tau}_{ij}}{\partial x_j} \tag{1}$$

$$\frac{\partial(\rho\bar{u}_i)}{\partial x_i} = 0 \tag{2}$$

where ρ is the density, \bar{u}_i is the averaged velocity vector, $\overline{\rho u'_i u'_j}$ is the Reynolds stress tensor, \bar{p} is the mean pressure and $\bar{\tau}_{ij}$ is the mean viscous stress tensor, given as:

$$\bar{\tau}_{ij} = \mu \left(\frac{\partial \bar{u}_i}{\partial x_j} + \frac{\partial \bar{u}_j}{\partial x_i} \right) \tag{3}$$

where μ is the dynamic viscosity coefficient.

In order to close Equations (1) and (2), $k - \omega$ SST turbulence model with wall functions is applied. For the discretization of governing equations, the finite volume method (FVM) is utilized, and the volume of fluid (VOF) method with high resolution interface capturing (HRIC) is utilized for tracking and locating the free surface. After the discretization, Equations (1) and (2) are solved in a segregated manner, the second order upwind convection scheme is used for the discretization of convective terms, while temporal discretization is performed using the first order scheme.

As already noted, the impact of roughness, i.e., biofouling, can be noticed as a downward shift of the mean velocity profile within the log-law region of TBL:

$$U^+ = \frac{1}{\kappa} \ln y^+ + B - \Delta U^+ \tag{4}$$

where κ is the von Karman constant, U^+ is the non-dimensional mean velocity, y^+ is the non-dimensional normal distance from the wall and B is the smooth wall log-law intercept.

The drag characterization of a certain roughness or fouling type means finding the relation between ΔU^+ and k^+ , where k^+ is defined as:

$$k^+ = \frac{k u_\tau \rho}{\mu} \tag{5}$$

where k is the roughness length scale, which cannot be directly measured.

Schultz has proposed following scaling for the hard fouling [12]:

$$k = 0.059 R_t \sqrt{\%SC}, \tag{6}$$

where R_t is the height of the largest barnacles, while $\%SC$ is the percentage of the surface covered with barnacles.

Using Equation (6), Schultz has demonstrated excellent collapse for the obtained results with the Grigson roughness function, which is given with following equation:

$$\Delta U^+ = \frac{1}{\kappa} \ln(1 + k^+) \tag{7}$$

It should be noted that Schultz has proposed Equation (6) based on the assumption that the height of the larger barnacles has the dominant influence on drag and that the effect of increase in %SC is larger for lower %SC and smaller for higher %SC, and these assumptions were deduced from the obtained results, pipe flow experiments [23] and the observations from [24] for typical roughness types.

An explanation of the approach for the determination of the impact of biofilm on the ship resistance and propulsion characteristics is presented in [8,18] and is applied within this study. Firstly, an experimental study related to towing tank measurements of fouled flat plates was carried out within [12]. Based on the obtained results, Schultz has proposed Equation (6) for the determination of roughness length scale and Equation (7) as a ΔU^+ model for hard fouling. This ΔU^+ model was implemented within the wall function of CFD solver and CFD model was validated with the comparison of the numerically obtained frictional resistance coefficients for fouled flat plates [16] with the experimentally measured ones [12]. Additionally, CFD simulations for fouled full-scale plates representing two merchant ships were carried out, and the obtained results were compared with the results obtained using Granville similarity law scaling method [16]. Once the CFD model is validated, it can be utilized for the assessment of the impact of hard fouling on the resistance and propulsion characteristics. The impact of hard fouling on the ship resistance characteristics for two merchant ships is studied in [16] using CFD simulations of a towed ship. In this paper, the impact of hard fouling on the propeller performance in open water conditions is assessed through implementation of ΔU^+ model for hard fouling within wall function of CFD solver and by performing CFD simulations of the open water test (OWT). CFD simulations of OWT are performed using the moving reference frame (MRF) method, and CFD simulations are performed as steady simulations. More details regarding this method can be found within [25]. The impact of hard fouling on ship propulsion characteristics is assessed utilizing the proposed ΔU^+ model within CFD simulations of the self-propulsion test (SPT). It should be noted that CFD simulations of SPT are performed using the body force method and more details regarding this method can be found in [25]. The change in certain hydrodynamic characteristic is calculated as follows:

$$\Delta\varphi = \frac{\varphi_R - \varphi_S}{\varphi_S} \cdot 100\% \tag{8}$$

where φ_R represents certain hydrodynamic characteristic for fouled condition and φ_S represents certain hydrodynamic characteristic for smooth surface condition.

The impact of hard fouling on the ship performance is studied for six different fouling conditions presented in Table 1. The presented fouling conditions are investigated considering certain fouling condition present both at the hull and propeller.

Table 1. Studied fouling conditions.

Fouling Condition	$R_t, \mu\text{m}$	%SC, %	$k, \mu\text{m}$
R1	7000	25	2065
R2	5000	25	1475
R3	7000	5	923.5
R4	5000	5	659.64
R5	7000	1	413
R6	5000	1	295

2.2. Resistance, Open Water and Propulsion Characteristics

The total resistance coefficient can be decomposed as follows:

$$C_T = (1 + k)C_F + C_W \quad (9)$$

where k represents the form factor, C_F represents the frictional resistance coefficient and C_W represents the wave resistance coefficient. It should be noted that C_T is obtained by dividing total resistance (R_T) with $\frac{1}{2}\rho v^2 S$ (where v is the ship speed and S is the wetted surface) and in that way, the non-dimensional form is obtained.

Effective power (P_E) can be obtained as a product of R_T and v . Most studies related to the impact of biofouling on ship performance investigate the effect of biofouling on effective power. However, the fuel consumption and greenhouse gas (GHG) emission can be related to delivered power (P_D) and propeller rotation rate (n). The quasi-propulsive efficiency coefficient defines relation between P_E and P_D as follows:

$$\eta_D = \frac{P_E}{P_D} = \eta_H \eta_O \eta_R \quad (10)$$

where η_H is the hull efficiency, η_O is the open water efficiency and η_R is the relative rotative efficiency. These efficiencies are defined as follows:

$$\eta_H = \frac{1 - t}{1 - w} \quad (11)$$

$$\eta_O = \frac{J}{2\pi} \frac{K_{TO}}{K_{QO}} \quad (12)$$

$$\eta_R = \frac{K_{QO}}{K_Q} \quad (13)$$

where t is the thrust deduction coefficient, w is the wake fraction coefficient, J is the advance coefficient, K_{TO} is the thrust coefficient in open water conditions, K_{QO} is the torque coefficient in open water conditions and K_Q is the torque coefficient obtained in SPT.

Delivered power can be obtained as follows:

$$P_D = 2\pi \rho K_Q n^3 D^5 \quad (14)$$

where D is the propeller diameter.

3. Computational Model

3.1. Case Study

Within this paper, the impact of hard fouling on the ship performance is presented on the example of three commercial ships: containership, oil tanker and bulk carrier. The portion of CO₂ emission from containerships, bulk carriers and tankers in total CO₂ emission from international shipping is significantly higher than for other ship types and accounts for almost 62% of CO₂ emission from international shipping [26]. The Kryo Container Ship (KCS) was designed with an aim to represent a modern panamax container ship with a bulbous bow [27]. The Korea Research Institute for Ships and Ocean Engineering (KRISO) carried out an extensive towing tank experiments, in order to determine resistance, mean flow data and free surface waves [27]. Self-propulsion tests were performed at the Ship Research Institute (now the National Maritime Research Institute, NMRI) in Tokyo, and the obtained results were reported in the Proceedings of the CFD Workshop Tokyo in 2005 [28]. Kryo Very Large Crude-oil Carrier 2 (KVLCC2) was designed with the aim to represent a large oil tanker that can transport 300,000 t of crude oil, and it represents the second variant of KRISO tanker with more U-shaped stern frame lines in comparison with KVLCC. KRISO carried out resistance and self-propulsion tests,

as well as towing tank measurements for the determination of mean flow data and wave profile elevations [27]. Bulk Carrier (BC) represents a typical handymax bulk carrier. Extensive towing tank experiments, including resistance tests, self-propulsion tests, as well as nominal wake measurements were performed in Brodarski institute [29]. It should be noted that KCS, KVLCC2 and BC were only designed as models, i.e., full-scale ships have never been built. The geometry of the investigated ships is presented in Figure 1.

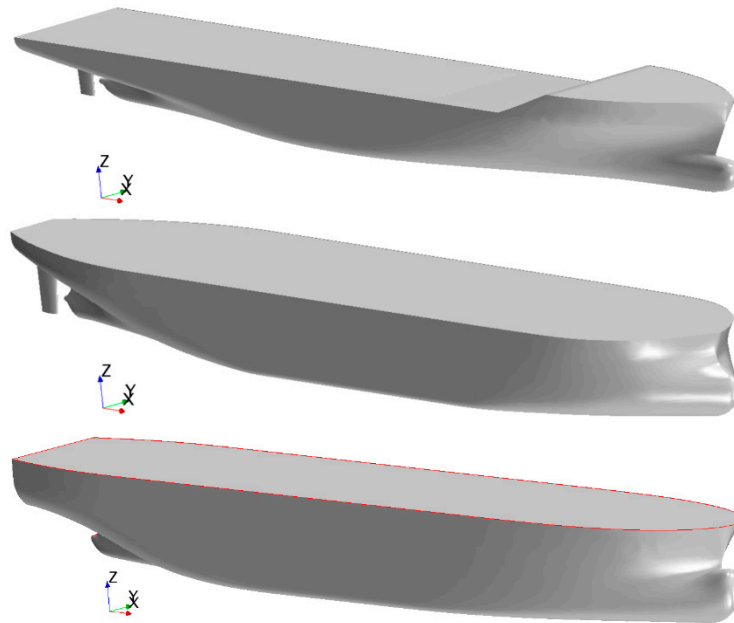


Figure 1. Geometry of the Kriso Container Ship (KCS) (upper), Kriso Very Large Crude-oil Carrier 2 (KVLCC2) (middle) and Bulk Carrier (BC) (lower).

From Figure 1, it is evident that all three ships have bulbous bow and transom stern. KCS has more slender form than BC and KVLCC2. The main particulars of the investigated ships are presented in Table 2.

Table 2. The main particulars of KCS, KVLCC2 and BC.

Parameter	KCS	KVLCC2	BC
length between perpendiculars, L_{pp}	230 m	320 m	175 m
waterline length, L_{wl}	232.5 m	325.5 m	182.69 m
breadth, B	32.2 m	58 m	30 m
draft, T	10.8 m	20.8 m	9.9 m
Displacement, Δ	53,382.8 t	320,750 t	41,775 t
Displacement volume, ∇	52,030 m ³	312,622 m ³	40,716 m ³
Wetted surface, S	9645 m ²	27,467 m ²	7351.9 m ²
Block coefficient, C_B	0.6505	0.8098	0.7834
Froude number, F_n	0.26	0.1423	0.2026
Design speed, V	24 kn	15.5 kn	16.32 kn
Propeller center, longitudinal location from FP (x/L_{pp})	0.9825	0.9797	0.9800
Propeller center, vertical location from WL ($-z/T$)	0.62037	0.72115	0.6800

SPT were performed using the KP505 for KCS, the KP458 for KVLCC2 and one stock propeller from the Wageningen series (WB) for BC, and their geometry is shown in Figure 2. The main particulars of the investigated propellers are given in Table 3. Towing tank tests for all three investigated propellers are performed at Reynolds numbers (Rn) higher than $Rn = 2 \cdot 10^5$ as prescribed by ITTC [30], and the obtained results are given in [29,31,32].



Figure 2. KP505 (left), KP458 (middle) and Wageningen series (WB) (right) propeller.

Table 3. The main particulars of KP505, KP458 and WB.

Propeller	KP505	KP458	WB
propeller diameter, D	7.900 m	9.860 m	6.199 m
propeller pitch, P	7.505 m	7.085 m	5.294 m
number of blades, Z	5	4	4
chord length, c	2.844 m	2.233 m	1.633 m
maximum thickness of profile, t	0.132 m	0.131 m	0.168 m
Hub ratio, d/D	0.180	0.155	0.179

3.2. Computational Domain and Boundary Conditions

In this study, the impact of hard fouling on resistance, open water and propulsion characteristics is investigated using CFD simulations of resistance, open water and self-propulsion tests. It should be noted that the impact of hard fouling on resistance characteristics of KCS and KVLCC2 is already investigated in [16]. Therefore, within this paper, the impact of hard fouling on ship resistance characteristics is only briefly presented as it is important for further discussion. R_T of a ship is determined using CFD simulations which include free surface effects, i.e., free surface simulations (FSS). Viscous resistance (R_V) is obtained using double body simulations (DBS), which do not take free surface effects into account. In DBS, the flow around deeply immersed double body ship is simulated and thus the obtained R_T is equal to R_V . The frictional resistance (R_F) is obtained by integrating the tangential stresses over the wetted surface, while viscous pressure resistance (R_{VP}) is obtained by integrating the pressure over the wetted surface in DBS. Once R_V and R_F are determined, $1 + k$ is determined as a ratio between R_V and R_F . Wave resistance (R_W) is obtained as difference between R_T obtained in FSS and R_V obtained in DBS. For more details regarding the performed CFD simulations of resistance tests, reference may be given to [16]. It should be noted that CFD simulations of resistance tests for BC are performed using the same computational domain and boundary conditions as in [16]. CFD simulations of OWT are performed using the cylindrical computational domain. The domain boundaries are placed sufficiently far from the investigated propeller and appropriate boundary conditions are applied in order to prevent their impact on the obtained solution, Figure 3. The computational domain for CFD simulations of SPT is the same as for CFD simulations of resistance test, however within CFD simulations of SPT symmetry condition is not applied, i.e., the whole computational domain is generated (Figure 4). In Figure 4, the applied boundary conditions are presented as well. It should be noted that the same boundary conditions are applied in CFD simulations of the resistance test, except for the symmetry boundary condition, which is applied at the symmetry plane within CFD simulations of resistance test. Possible occurrence of wave reflection is prevented by applying VOF wave damping at the inlet, outlet and side boundaries. More details regarding the applied damping function can be found in [33], and the VOF wave damping length is set to L_{pp} .

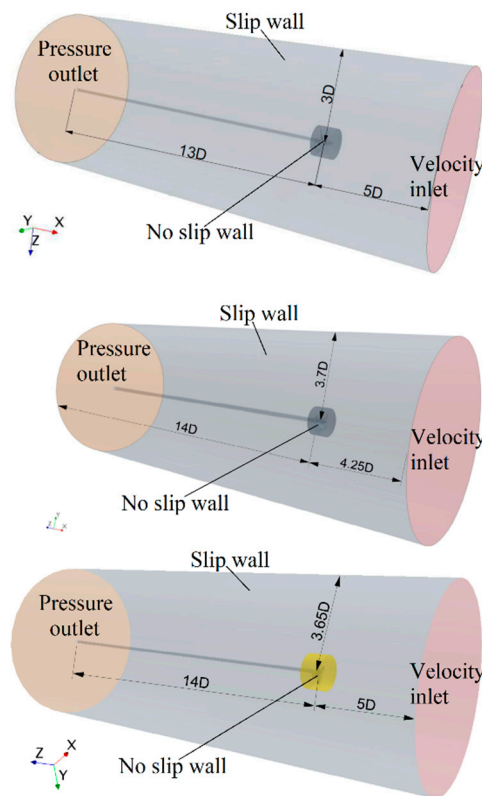


Figure 3. Computational domain for the open water test (OWT): KP505 (upper), KP458 (middle) and WB (lower).

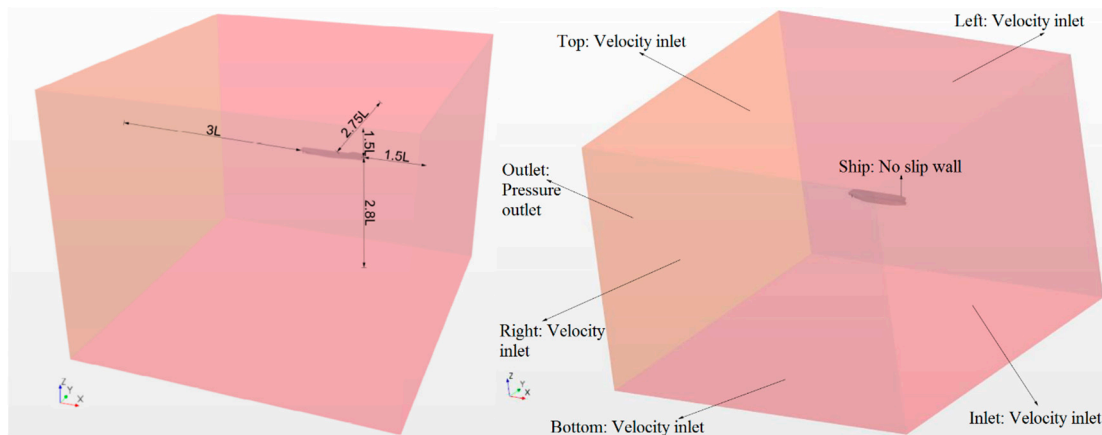


Figure 4. Computational domain (left) and the applied boundary conditions (right) within computational fluid dynamics (CFD) simulations of the self-propulsion test (SPT).

3.3. Discretization of Computational Domain and Computational Setup

Cut-cell grids with prism layer mesh on the walls were made utilizing the surface remesher, prism layer mesher and trimmer mesher within STAR-CCM+. The unstructured hexahedral mesh is refined locally in the critical regions. Thus, within DBS and FSS of resistance test, as well as in CFD simulations of SPT, mesh is refined near the hull surface, near the bow and stern and hull surface is discretized very fine, i.e., the cell size at the hull surface is set to $1/1000 L_{pp}$. Within CFD simulations including free surface effects, mesh is refined in the region where free surface is expected, as well as in order to capture Kelvin wake around free surface. Additionally, mesh for CFD simulations of SPT is refined in the region where virtual disk is located. It should be noted that refinements are made in the same way within [8,25,34]. The mesh for CFD simulations of OWT is refined in the region around the propeller.

Additionally, mesh is particularly refined along the leading and trailing edges of propeller in order to allow proper demarcation between the suction and pressure sides. The thickness of the first cell on the wall surfaces within all CFD simulations is chosen in a way that y^+ values are higher than 30 and k^+ values, as recommended by [15]. As a result of this, near wall mesh for smooth and fouled surfaces is not the same since investigated surface conditions represent very severe fouling conditions with high k values. The obtained mesh for CFD simulations of OWT is presented in Figure 5, while the obtained mesh for CFD simulations of SPT is shown in Figure 6. Within these two figures, the above mentioned refinements can be seen.

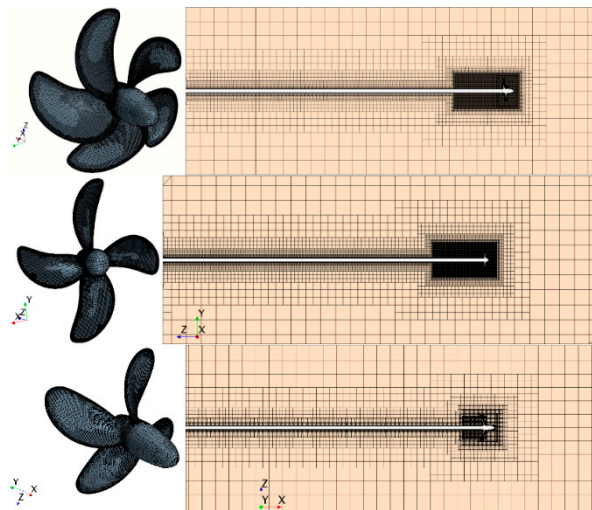


Figure 5. Propeller surface (left) and profile view (right) cross section of the volume mesh for KP505 (upper), KP458 (middle) and WB (lower).

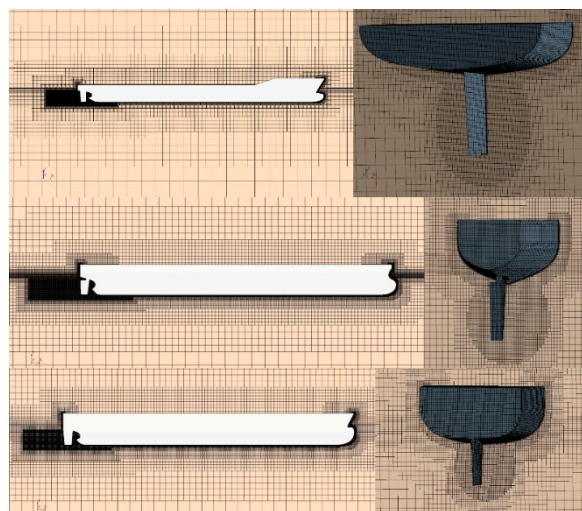


Figure 6. The profile view cross-section of the domain for KCS (upper left), KVLCC2 (middle left) and BC (lower left) and mesh refinement in stern region of KCS (upper right), KVLCC2 (middle right) and BC (lower right).

CFD simulations of OWT are performed for full-scale KP505, KP458 and WB in a way that $n = 1.5$ rps is kept constant and advance velocity varies with J . CFD simulations for KP505 are performed for range of J from 0.1 to 0.8, with a step equal to 0.1, for KP458 for range of J from 0.1 to 0.7 with step equal to 0.1 and for WB for range of J from 0.08 to 0.88 with step equal to 0.08. CFD simulations of SPT are performed without discretization of propeller geometry, as the body force method is applied. Therefore, a virtual disk model is placed at the propeller location with the inner

radius of the virtual disk set to the propeller hub radius and the outer radius set to the propeller radius (R). Thickness of virtual disk model is set as propeller thickness, the inflow plane radius is set as $1.1R$ and the inflow plane offset is set as $2.2R$ towards the bow from the half of virtual disk thickness.

CFD simulations without free surface effects, i.e., DBS of resistance test and CFD simulations of OWT, are performed as steady simulations. The remaining CFD simulations include free surface effect, and they are performed with time step equal to $T/200$, where T is the ratio between L_{pp} and ship speed (v). FSS of resistance test and CFD simulations of SPT are stopped once R_T and thrust (T) force became steady, i.e., once they oscillate around averaged value with oscillation amplitude lower than 0.5% of R_T or T value.

4. Verification and Validation Study

4.1. Verification Study

A verification study is carried out in order to estimate sufficient grid spacings and adequate time steps. This study is carried out using three different meshes and three different time steps. Verification study for grid size is made with fine time step and verification study for time step is made with fine mesh. Thereafter, numerical uncertainty, which is consisted of both spatial and temporal uncertainties, is calculated using the grid convergence index (GCI) method. This method is recommended by the American Society of Mechanical Engineers, as well as by the American Institute of Aeronautics and Astronautics for the assessment of grid uncertainty (U_G) [35], but can be used for the assessment of temporal uncertainty (U_T) as well [35–37]. More details regarding the GCI method and numerical uncertainty can be found in [18].

For the purposes of verification study three meshes are generated for smooth surface condition and fouling condition R1. Since all mesh parameters, except prism layer mesh, are set to be relative to cell base size, mesh is refined by changing cell base size. It should be noted that all remaining CFD simulations, i.e., for the fouling conditions R2, R3, R4, R5 and R6 are performed using fine mesh. In Table 4, the number of cells used in the verification study is shown. Three different time steps, i.e., $T/50$, $T/100$ and $T/200$ are used in the verification study for time step.

Table 4. Number of cells within CFD simulations.

Smooth Surface Condition			
Simulation	KCS/KP 505	KVLCC2/KP 458	BC/WB
	Coarse/Medium/Fine	Coarse/Medium/Fine	Coarse/Medium/Fine
OWT	3.50/5.10/7.10 Million	2.40/3.30/5.30 Million	2.20/3.50/5.00 Million
SPT	2.12/4.19/8.47 Million	1.23/2.74/5.25 Million	0.96/2.20/5.06 Million
Fouling Condition R1			
Simulation	KCS/KP 505	KVLCC2/KP 458	BC/WB
	Coarse/Medium/Fine	Coarse/Medium/Fine	Coarse/Medium/Fine
OWT	2.30/3.50/5.30 Million	1.80/2.30/3.90 Million	1.60/2.40/3.40 Million
SPT	1.89/3.83/7.54 Million	1.14/2.54/4.86 Million	0.89/2.01/4.61 Million

It should be noted that the verification study for CFD simulations of resistance tests of KCS and KVLCC2 is carried out in [16]. Numerical uncertainties in the prediction of R_F and R_V consisted of grid uncertainties solely, and R_T consisted of grid and temporal uncertainties, which are calculated using the GCI method. The obtained numerical uncertainties in the prediction of R_F were below 1.3% for both ships and for all analyzed fouling conditions (Table 1). Numerical uncertainties in the prediction of R_V were slightly higher, however, the highest obtained numerical uncertainty was equal to 2.86%. Finally, the highest numerical uncertainties are obtained for the prediction of R_T . Nevertheless, these grid and time step uncertainties were relatively low, i.e., the highest obtained grid uncertainty in the

prediction of R_T was equal to 2.99%, while the highest time step uncertainty in the prediction of R_T was equal to 0.1%. Within this paper, the numerical uncertainty in the prediction of K_{TO} and $10K_{QO}$ from CFD simulations of OWT are calculated for one J value and the obtained results are presented in Tables 5 and 6. Additionally, numerical uncertainty in the prediction of P_D , n , T and J from CFD simulations of SPT are calculated.

Table 5. The verification study for K_{TO} .

Propeller	J	ϕ_3	ϕ_2	ϕ_1	ϕ_{ext}^{21}	GCI_{fine}^{21} %
KP505 S	0.7	0.18068	0.18047	0.18058	0.18071	0.092
KP458 S	0.5	0.18513	0.18576	0.18478	0.18264	1.443
WB S	0.56	0.17468	0.17338	0.17250	0.16758	3.565
KP505 R1	0.6	0.20722	0.20665	0.20668	0.20668	0.001
KP458 R1	0.4	0.15868	0.15883	0.15725	0.15698	0.217
WB R1	0.4	0.20876	0.20855	0.20878	0.21098	1.317

Table 6. The verification study for K_{QO} .

Propeller	J	ϕ_3	ϕ_2	ϕ_1	ϕ_{ext}^{21}	GCI_{fine}^{21} %
KP505 S	0.7	0.29436	0.29386	0.29387	0.29387	0.000
KP458 S	0.5	0.21219	0.21268	0.21169	0.21045	0.729
WB S	0.56	0.24312	0.24120	0.23910	0.23372	2.815
KP505 R1	0.6	0.40234	0.40168	0.40249	0.40615	1.136
KP458 R1	0.4	0.22703	0.22713	0.22533	0.22512	0.115
WB R1	0.4	0.32578	0.32591	0.32531	0.32524	0.024

As can be seen from Tables 5 and 6, relatively low numerical uncertainties are obtained, and are in line with numerical uncertainties of other CFD studies regarding open water tests [38,39]. Thus, the highest U_G in the prediction of K_{TO} and $10K_{QO}$ is obtained for the WB propeller with smooth surface condition, and it is equal to 3.565% and 2.815%, respectively. It should be noted that numerical uncertainties obtained for smooth and fouled propellers are relatively close, i.e., numerical uncertainty has not raised due to the roughness effects.

From the results of verification study of SPT, Tables 7–9, it can be concluded that U_T are lower than U_G . Generally, the obtained U_G related to the prediction of P_D for smooth and fouled ships are slightly higher than for the other investigated key variables and the highest GCI_{fine}^{21} for KCS is equal to 3.123%, for KVLCC2 is equal to 1.174% and for BC is equal to 7.318%. The obtained U_T related to the prediction of P_D for smooth and fouled ships are lower and the highest GCI_{fine}^{21} for KCS is equal to 1.366%, for KVLCC2 is equal to 1.502% and for BC is equal to 3.390%. The obtained U_G related to the prediction of n for smooth and fouled ships are the lowest amongst investigated key variables and the highest GCI_{fine}^{21} for KCS is equal to 0.255%, for KVLCC2 is equal to 0.164% and for BC is equal to 1.661%. Interestingly, the obtained U_T values related to the prediction of n for smooth and fouled ships are higher than U_G values and the highest U_T for KCS is equal to 0.401%, for KVLCC2 is equal to 0.701% and for BC is equal to 2.909%. The obtained U_G values related to the prediction of T for smooth and fouled ships are low and the highest GCI_{fine}^{21} for KCS is equal to 3.273%, for KVLCC2 is equal to 1.478% and for BC is equal to 4.717%. The obtained U_T values related to the prediction of T for smooth and fouled ships are lower or similar to U_G and the highest GCI_{fine}^{21} for KCS is equal to 0.807%, for KVLCC2 is equal to 1.529% and for BC is equal to 3.499%. Finally, the obtained U_G values related to the prediction of J for smooth and fouled ships are low and the highest GCI_{fine}^{21} for KCS is equal to 0.452%, for KVLCC2 is equal to 1.257% and for BC is equal to 2.041%. The obtained U_T values related to the prediction of J for smooth and fouled ships are low as well, and the highest GCI_{fine}^{21} for KCS is equal to 0.451%, for KVLCC2 is equal to 0.703% and for BC is equal to 2.719%.

Table 7. The obtained grid uncertainties in the prediction of P_D , n , T and J .

P_D							
Ship	Surface Condition	ϕ_3 , MW	ϕ_2 , MW	ϕ_1 , MW	ϕ_{ext}^{21} , MW	GCI_{fine}^{21} , %	U_G , MW
KCS	S	26.744	25.321	24.624	24.009	3.123	0.769
	R1	67.008	65.429	64.807	64.361	0.860	0.558
KVLCC2	S	20.172	17.325	17.850	18.017	1.174	0.209
	R1	58.651	55.524	55.940	56.036	0.214	0.120
BC	S	7.384	7.267	6.725	6.573	2.825	0.190
	R1	20.778	21.326	20.301	19.112	7.318	1.486
n							
Ship	Surface Condition	ϕ_3 , rpm	ϕ_2 , rpm	ϕ_1 , rpm	ϕ_{ext}^{21} , rpm	GCI_{fine}^{21} , %	U_G , rpm
KCS	S	100.982	99.686	99.341	99.225	0.146	0.145
	R1	118.374	117.672	117.376	117.137	0.255	0.299
KVLCC2	S	73.068	70.484	70.858	70.951	0.164	0.117
	R1	95.356	93.902	93.963	93.968	0.007	0.006
BC	S	101.830	101.580	99.541	99.251	0.364	0.362
	R1	130.805	132.033	131.120	128.345	1.661	2.160
T							
Ship	Surface Condition	ϕ_3 , kN	ϕ_2 , kN	ϕ_1 , kN	ϕ_{ext}^{21} , kN	GCI_{fine}^{21} , %	U_G , kN
KCS	S	1903.77	1877.34	1810.89	1763.46	3.273	59.281
	R1	3669.43	3630.48	3605.91	3557.73	1.670	60.226
KVLCC2	S	2276.43	2015.69	2009.71	2009.41	0.019	0.374
	R1	4557.62	4308.72	4390.60	4442.50	1.478	64.872
BC	S	829.63	813.35	763.94	739.27	4.037	30.839
	R1	1616.88	1644.82	1592.13	1532.04	4.717	75.107
J							
Ship	Surface Condition	ϕ_3	ϕ_2	ϕ_1	ϕ_{ext}^{21}	GCI_{fine}^{21} , %	U_G
KCS	S	0.7196	0.7215	0.7293	0.7319	0.452	0.0033
	R1	0.5476	0.5442	0.5452	0.5456	0.094	0.001
KVLCC2	S	0.4428	0.4603	0.4573	0.4564	0.248	0.0011
	R1	0.3066	0.3128	0.3099	0.3068	1.257	0.0039
BC	S	0.5160	0.5209	0.5328	0.5414	1.997	0.0106
	R1	0.3593	0.3580	0.3591	0.3649	2.041	0.0073

The obtained U_T , U_Q , U_n , U_{P_D} and U_J , which consist of both U_G and U_T , are shown in Table 9. As can be seen from Table 9, the lowest U_{SN} values for smooth and fouled ships are obtained for KCS, which was expected, since U_G values are higher than U_T values and the mesh for KCS had more cells than for KVLCC2 and BC. The highest U_{SN} is obtained for the prediction of U_{P_D} for BC fouled with R1 and it is equal to 7.421% and other obtained U_{SN} values are lower than 5.5%. Higher U_{P_D} were expected, since, for the prediction of P_D , both n and the propeller torque should be determined. It should be noted that the obtained U_{P_D} are in line with the previously published studies [8,25]. From Table 9, it can be seen that higher numerical uncertainties are obtained for the prediction of P_D and T , than for n and J , which was also obtained in [8]. Additionally, it can be seen that U_{SN} in the prediction of key variables for R1 are mostly below U_{SN} for smooth surface condition. Higher U_{SN} obtained for R1 than for smooth surface condition can be ascribed to the lower cell number used in CFD simulations of SPT for rough surface condition (Table 4). Therefore, it can be concluded that the implementation of ΔU^+ within the wall function did not cause higher uncertainties in the prediction of the key variables.

Table 8. The obtained temporal uncertainties in the prediction of P_D , n , T and J .

P_D							
Ship	Surface Condition	ϕ_3 , MW	ϕ_2 , MW	ϕ_1 , MW	ϕ_{ext}^{21} , MW	GCI_{fine}^{21} , %	U_T , MW
KCS	S	25.058	24.918	24.624	24.355	1.366	0.336
	R1	65.020	65.198	64.807	64.479	0.633	0.410
KVLCC2	S	17.413	17.256	17.850	18.064	1.502	0.268
	R1	56.335	55.490	55.940	56.454	1.147	0.642
BC	S	6.813	6.903	6.725	6.542	3.390	0.228
	R1	20.546	20.458	20.301	20.101	1.233	0.250
n							
Ship	Surface Condition	ϕ_3 , rpm	ϕ_2 , rpm	ϕ_1 , rpm	ϕ_{ext}^{21} , rpm	GCI_{fine}^{21} , %	U_T , rpm
KCS	S	99.697	99.577	99.341	99.094	0.311	0.309
	R1	117.477	117.628	117.376	116.999	0.401	0.471
KVLCC2	S	70.490	70.249	70.858	71.255	0.701	0.496
	R1	94.492	93.715	93.963	94.079	0.154	0.145
BC	S	99.638	100.066	99.541	97.225	2.909	2.896
	R1	130.805	130.529	130.073	129.374	0.672	0.874
T							
Ship	Surface Condition	ϕ_3 , kN	ϕ_2 , kN	ϕ_1 , kN	ϕ_{ext}^{21} , kN	GCI_{fine}^{21} , %	U_T , kN
KCS	S	1833.25	1827.69	1810.89	1802.58	0.574	10.388
	R1	3611.92	3621.12	3605.91	3582.67	0.807	29.104
KVLCC2	S	2025.11	2018.75	2009.71	1988.26	1.334	26.816
	R1	4371.42	4347.51	4390.60	4444.32	1.529	67.146
BC	S	774.04	784.54	763.94	742.56	3.499	26.730
	R1	1609.60	1597.42	1592.13	1588.07	0.319	5.077
J							
Ship	Surface Condition	ϕ_3	ϕ_2	ϕ_1	ϕ_{ext}^{21}	GCI_{fine}^{21} , %	U_T
KCS	S	0.7269	0.7279	0.7293	0.7319	0.451	0.0033
	R1	0.5457	0.5442	0.5452	0.5466	0.335	0.0018
KVLCC2	S	0.4596	0.4600	0.4573	0.4569	0.114	0.0005
	R1	0.3107	0.3116	0.3099	0.3082	0.703	0.0022
BC	S	0.5312	0.5276	0.5328	0.5444	2.719	0.0145
	R1	0.3590	0.3590	0.3591	0.3591	0.007	0.0000

Table 9. The obtained simulation uncertainties (U_{SN}) in the prediction of P_D (U_{P_D}), n (U_n), T (U_T) and J (U_J).

Ship	KCS		KVLCC2		BC	
Surface condition	U_{P_D} , MW	U_{P_D} , %	U_{P_D} , MW	U_{P_D} , %	U_{P_D} , MW	U_{P_D} , %
S	0.839	3.409	0.340	1.906	0.297	4.413
R1	0.692	1.068	0.653	1.167	1.506	7.421
Surface condition	U_n , rpm	U_n , %	U_n , rpm	U_n , %	U_n , rpm	U_n , %
S	0.341	0.343	0.510	0.720	2.918	2.932
R1	0.558	0.475	0.145	0.154	2.331	1.791
Surface condition	U_T , kN	U_T , %	U_T , kN	U_T , %	U_T , kN	U_T , %
S	60.185	3.323	26.819	1.334	60.185	3.323
R1	66.890	1.855	93.365	2.126	66.890	1.855
Surface condition	U_J	U_J , %	U_J	U_J , %	U_J	U_J , %
S	0.0047	0.638	0.0012	0.273	0.0180	3.374
R1	0.0019	0.348	0.0045	1.440	0.0073	2.041

4.2. Validation Study

Relative deviations between numerically obtained and extrapolated results are calculated using the following equation:

$$RD = \frac{\phi_{CFD} - \phi_{EX}}{\phi_{EX}} \cdot 100\% \tag{15}$$

where ϕ_{CFD} is the certain hydrodynamic characteristic obtained using CFD and ϕ_{EX} is the certain hydrodynamic characteristic obtained using the ITTC 1978 Performance Prediction Method (PPM) and experimental results [30].

The obtained C_T for full-scale KCS and KVLCC2 is validated within [16] through comparison of the obtained numerical results with extrapolated values using original ITTC 1978 PPM, based on Equation (9). Within ITTC 1978 PPM, C_F is determined using the ITTC 1957 model-ship correlation line. In Table 10, the validation of the numerically obtained C_T for the smooth surface condition is presented. As can be seen from Table 10, the obtained results are in satisfactory agreement with the extrapolated results, i.e., the highest RD is obtained for BC and it is equal to -4.338% .

Table 10. The validation study for C_T .

Ship	C_T		RD, %
	CFD	EX	
KCS [16]	2.081	2.053	1.376
KVLCC2 [16]	1.795	1.724	4.107
BC	2.197	2.296	-4.338

The numerically obtained open water characteristics for all three propellers have been validated, with the towing tank results published in the literature [29,31,32]. It should be noted that CFD simulations of OWT are performed in full-scale, while experimental OWT are performed in model scale. Towing tank tests for all three investigated propellers are performed at Rn above $Rn = 2 \cdot 10^5$, as prescribed by ITTC [30]. In Figure 7, the comparison between the numerically and experimentally obtained open water characteristics is presented. From this figure, it can be seen that numerically obtained K_{TO} , $10K_{QO}$ and η_O are in satisfactory agreement with the experimentally obtained ones. Slightly higher RD between numerically and experimentally obtained K_{TO} and especially $10K_{QO}$ is obtained at lower J values, however, at higher J values, these RD are significantly lower.

The obtained results of the validation study for P_D and n are presented in Table 11, from which it can be concluded that satisfactory agreement is obtained. The highest obtained RD between numerical and extrapolated P_D is obtained for KVLCC2 and it is equal to -5.701% , while the highest obtained RD for n is obtained for BC and it is equal to -1.786% . The validation study for ship propulsion characteristics is presented in Table 12. From Table 12, it can be seen that the obtained RD for $1 - t$ are lower than 3.7% , for $1 - w$ are lower than 7.4% and for η_H are lower than 5.6% for all analyzed ships. It should be noted that slightly higher RD for $1 - w$ is obtained only for BC, and this can be attributed to the application of body force method. However, this RD is in line with previously published studies dealing with CFD simulations of SPT where the virtual disk model is applied [40,41]. The obtained RD for η_O are lower than 3.1% , for propeller efficiency behind ship (η_B) are lower than 3.8% , for η_R are lower than 2.9% and for η_D is lower than 6.2% . It should be noted that slightly higher RD for η_D is obtained only for KCS. However, in [42] where the authors carried out full-scale SPT for KCS using discretized propeller, η_D was equal to 0.766 , which is also lower than the extrapolated result. From this result, the obtained η_D in this paper has RD equal to -3.394% . In Table 12, the validation for the obtained J , K_T and K_Q for self-propulsion point is shown as well. It can be seen that the obtained RD for J are lower than 5.7% , for K_T are lower than 4.1% and for K_Q are lower than 3.4% for all analyzed ships. Generally, the obtained RD presented in Tables 11 and 12 can be ascribed to different reasons. For example, insufficiently precise assessment of the nominal wake, as well as the

propeller performance in OWT can be related to the inaccurate assessment of J for self-propulsion point, which then leads to inaccurate assessment of other propulsion characteristics. In addition to this, the modelling error should also be taken into account, as, in the body force method, the effect of propeller is modelled, rather than propeller itself. Furthermore, there is a numerical error as well, which is related to the applied mesh and time step. Lastly, there are also aspects regarding the applied PPM for the extrapolation of towing tank results. Namely, in [25] four different PPM are compared, and it was shown that extrapolated values can significantly vary with respect to the applied PPM. Thus, it was shown that for BC, extrapolated value of P_D can vary up to 1.5%, for n up to 0.4%, for $1 - t$ up to 0.5%, for $1 - w$ up to 6.3%, for η_R up to 1.1% and for η_B up to 2.6%. In addition to these variations, experimental uncertainty should also be considered. Considering all above mentioned aspects, it can be concluded that satisfactory agreement is achieved for P_D , n and all propulsion characteristics.

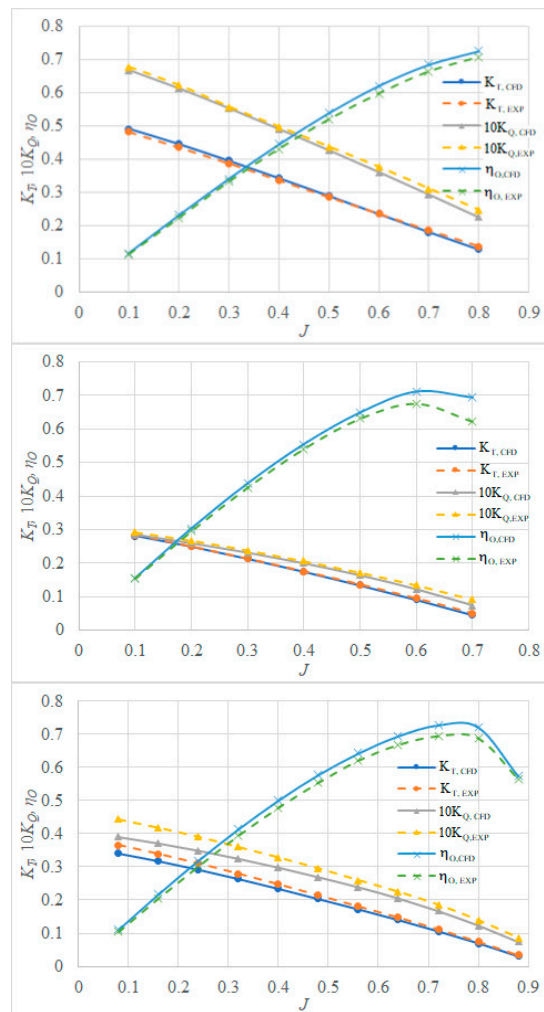


Figure 7. The validation study for open water characteristics of KP505 (upper), KP458 (middle) and WB (lower).

Table 11. The validation study for self-propulsion point.

Ship	n_{CFD} , rpm	n_{EX} , rpm	RD , %	$P_{D,CFD}$, MW	$P_{D,EX}$, MW	RD , %
KCS	99.341	100.359	-1.014	24.624	25.511	-3.476
KVLCC2	70.858	71.417	-0.784	17.850	18.929	-5.701
BC	99.541	101.351	-1.786	6.725	6.961	-3.392

Table 12. The validation study for propulsion characteristics.

Propulsion Characteristic	KCS		KVLCC2		BC	
	EX	CFD (RD,%)	EX	CFD (RD,%)	EX	CFD (RD,%)
$1 - t$	0.853	0.867 (1.613)	0.810	0.820 (1.199)	0.794	0.764 (-3.722)
$1 - w$	0.803	0.773 (-3.476)	0.695	0.668 (-3.904)	0.705	0.653 (-7.418)
η_H	1.062	1.122 (5.596)	1.165	1.227 (5.310)	1.126	1.171 (3.992)
η_O	0.690	0.700 (1.485)	0.620	0.600 (-3.146)	0.623	0.622 (-0.112)
η_B	0.698	0.702 (0.565)	0.623	0.600 (-3.752)	0.642	0.623 (-2.964)
η_R	1.011	1.002 (-0.906)	1.005	0.998 (-0.626)	1.030	1.000 (-2.855)
η_D	0.741	0.787 (6.193)	0.726	0.736 (1.359)	0.722	0.729 (0.910)
J	0.750	0.729 (-2.786)	0.472	0.457 (-3.145)	0.565	0.533 (-5.734)
K_T	0.161	0.165 (2.954)	0.155	0.149 (-4.055)	0.179	0.183 (2.312)
$10K_Q$	0.275	0.274 (-0.477)	0.187	0.180 (-3.449)	0.251	0.250 (-0.609)

5. The Impact of Hard Fouling on the Ship Performance

Within this section, the impact of hard fouling on the resistance, open water and propulsion characteristics is presented for three investigated ships. While detail investigation of the impact of hard fouling on resistance characteristics for KCS and KVLCC2 is presented in [16], within this study this impact is only briefly mentioned as emphasis is given to the impact of hard fouling on the ship performance, which is defined by propeller operating point.

5.1. The Impact of Hard Fouling on Resistance Characteristics

As demonstrated within [16,18] the impact of biofouling on each resistance component is different. Thus, the presence of biofouling causes the increase in C_F , decrease in C_W , while the impact of biofouling on $1 + k$ value is almost negligible. Consequently, it is valuable to study the increase in R_T , due to the presence of hard fouling through analysis of decomposed R_T and the portion of each resistance component in R_T for certain fouling condition. In Figure 8, decomposition of R_T for three investigated ships and fouling conditions is presented. Additionally, within Figure 8 the portions of R_F , R_{VP} and R_W in R_T are given. From Figure 8, it is clear that, for all analyzed ships, the portion of R_F in R_T increases, due to the presence of hard fouling, and this increase is the highest for KCS, which can be attributed to the ship speed. Namely, KCS is investigated at the highest speed and therefore u_τ values along the KCS hull are higher than u_τ values along the KVLCC2 and BC hulls. Since k^+ values and consequently ΔU^+ values for given fouling condition and fluid properties depend only on u_τ values, those values are higher for KCS than for KVLCC2 and BC resulting in higher increases in C_F [16]. Additionally, C_F for rough surface condition at high Rn value depends solely on k/L value, i.e., relative roughness [16]. The portion of R_{VP} in R_T due to the presence of hard fouling has increased for KCS and BC, while for KVLCC2 this portion has decreased. Regardless of this, from Figure 8, it is clear that the absolute value of R_{VP} , due to the presence of hard fouling, has increased, which is expected, since the impact

of biofouling on $1 + k$ value is minimal [16]. Finally, the portion of R_W in R_T due to the presence of hard fouling decreases for all analyzed ships and this decrease is the highest for KCS, which can be also attributed to ship speed. What is more, from Figure 8 it is clear that absolute values of R_W due to the presence of hard fouling have decreased for all analyzed ships [16]. Generally, KVLCC2 is the most affected, due to the presence of hard fouling in terms of the increase in R_T , which can be seen from Figure 9. Thus, the increase in R_T due to the presence of hard fouling for KVLCC2 ranges from 63.8% (R6) to 120.9% (R1), for BC ranges from 59.5% (R6) to 114.6% (R1) and for KCS ranges from 49.9% (R6) to 95.8% (R1). This can be mostly attributed to the portion of R_V in R_T , since, due to the presence of biofouling R_V , significantly increases. The portion of R_V in R_T is the highest for KVLCC2 and for smooth surface condition this portion is equal to 99.46%, as R_W of KVLCC2 is negligible [28]. However, beside the portion of R_V in R_T , the ship speed also affects the increase in R_T , as already explained. Thus, the increase in R_T due to the presence of hard fouling is only slightly lower for BC than for KVLCC2 and the portion of R_V in R_T for smooth surface condition is equal to 83.6%. It should be noted that the significantly lower increase in R_T is obtained for KCS, as KCS has relatively large portion of R_W in R_T (for smooth surface condition this portion is equal to 24.7%). Due to the presence of hard fouling, R_W decreases, and, therefore, the increase in R_T for KCS is lower.



Figure 8. Decomposition of R_T for KCS (upper), KVLCC2 (middle) and BC (lower) for smooth and fouled surface condition.

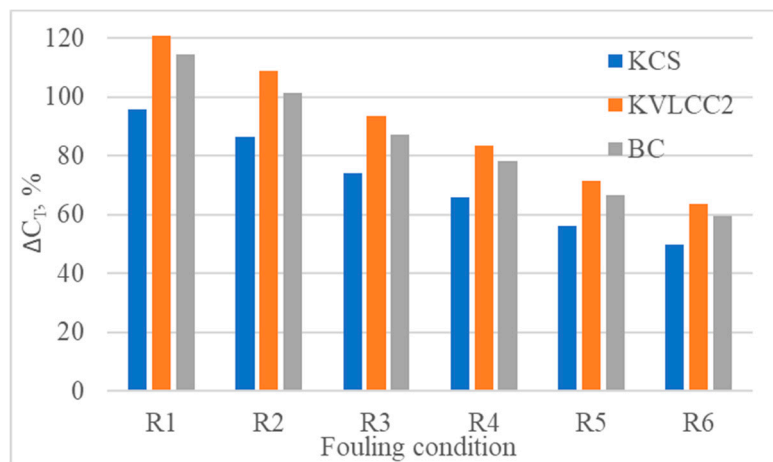


Figure 9. The impact of hard fouling on C_T .

5.2. The Impact of Hard Fouling on Open Water Characteristics

The impact of hard fouling (R1) on the propeller performance in open water conditions is presented in Figure 10. The obtained changes in K_{TO} , K_{QO} and η_O , due to the presence of hard fouling, are presented in Table 13. As can be seen from Figure 10 and Table 13, due to the presence of hard fouling K_{TO} has decreased and K_{QO} has increased resulting in significant reduction in η_O . As fouling severity increases (i.e., from R6 to R1), fouling penalties related to decrease in K_{TO} and increase in K_{QO} increase as well. Additionally, at higher J the fouling penalty related to decrease in η_O is higher. Therefore, it can be concluded that the ships operating at higher J values will experience a greater reduction in η_O , i.e., propeller fouling penalty on the ship performance will be greater. Thus, due to the presence of hard fouling ΔK_{TO} values for KP505 at $J = 0.6$ range from -6.22% (R6) to -12.05% (R1), for KP458 at $J = 0.4$ range from -7.44% (R6) to -14.45% (R1) and for WB at $J = 0.48$ range from -7.86% (R6) to -12.09% (R1). An increase in ΔK_{QO} values for KP505 at $J = 0.6$ range from 4.66% (R6) to 11.37% (R1), for KP458 at $J = 0.4$ range from 2.59% (R6) to 7.46% (R1) and for WB at $J = 0.48$ range from 3.77% (R6) to 11.19% (R1). Fouling penalties on the propeller performance in open water conditions can be ascribed to fouling impact on the skin friction and the pressure field. Thus, due to the presence of hard fouling on propeller surfaces wall shear stress (τ_w) increases, while the pressure difference between pressure and suction sides of propeller is reduced, which can be seen from Figures 11 and 12. In Figure 11, the obtained τ_w distributions at KP505 surface at $J = 0.7$ for both smooth and R1 surface condition are shown. It is clear that due to the presence of hard fouling τ_w values at KP505 surface are significantly increased resulting in increase in drag coefficient of the blade section and consequently in K_{QO} . In Figure 12 the obtained pressure distribution shown as distribution of pressure coefficient (C_p), which is defined as a ratio between pressure and $\frac{1}{2}\rho v_A^2$, at KP505 surface is presented. Since the magnitudes of C_p at both pressure and suction sides of fouled KP505 are significantly reduced, the pressure difference between pressure and suction sides is reduced as well, resulting in a decrease in the lift coefficient of the blade section and, consequently, in K_{TO} .

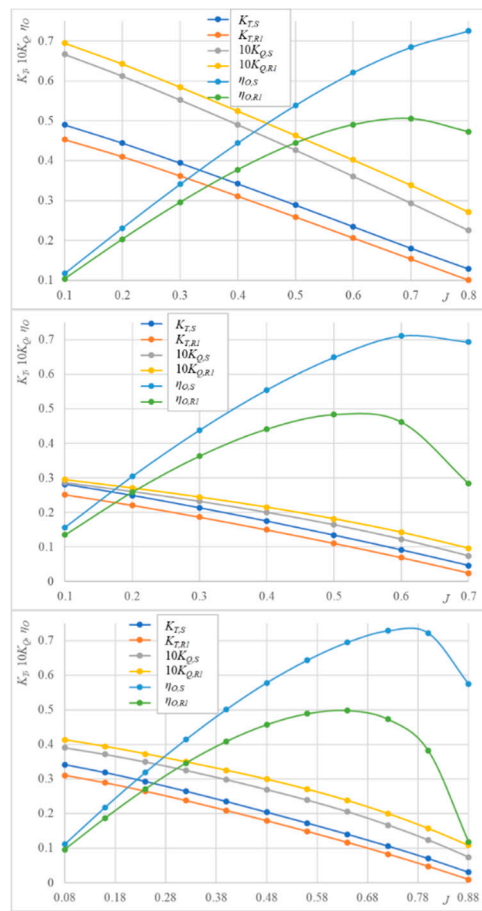


Figure 10. The impact of hard fouling (R1) on KP505 (upper), KP458 (middle) and WB (lower) performance in OWT.

Table 13. The obtained changes in K_{TO} , K_{QO} and η_O due to the presence of hard fouling.

Propeller	KP505			KP458			WB		
	$J = 0.6$			$J = 0.4$			$J = 0.48$		
Surface Condition	$\Delta K_{TO}, \%$	$\Delta K_{QO}, \%$	$\Delta \eta_O, \%$	$\Delta K_{TO}, \%$	$\Delta K_{QO}, \%$	$\Delta \eta_O, \%$	$\Delta K_{TO}, \%$	$\Delta K_{QO}, \%$	$\Delta \eta_O, \%$
R1	-12.05	11.37	-21.03	-14.45	7.46	-20.39	-12.09	11.19	-20.93
R2	-10.77	9.56	-18.55	-12.81	6.11	-17.83	-11.18	9.75	-19.07
R3	-9.24	7.66	-15.69	-11.66	4.69	-15.62	-10.10	7.65	-16.49
R4	-8.13	6.49	-13.73	-9.72	3.81	-13.03	-9.39	6.34	-14.79
R5	-6.85	5.30	-11.54	-8.20	2.99	-10.87	-8.47	4.75	-12.62
R6	-6.22	4.66	-10.39	-7.44	2.59	-9.77	-7.86	3.77	-11.21

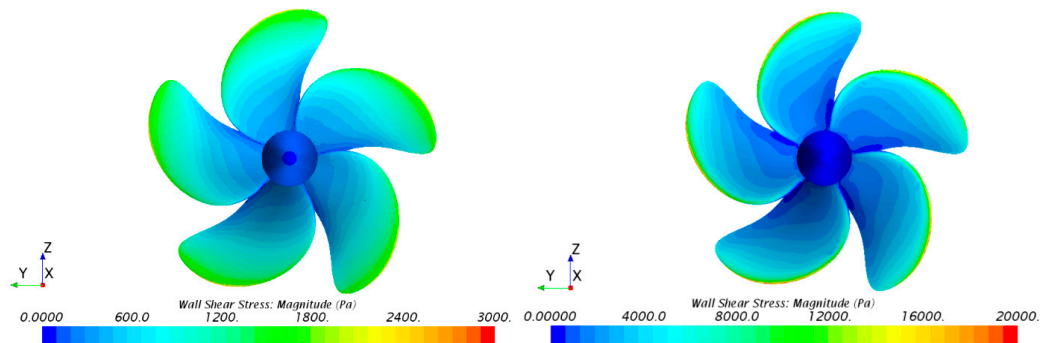


Figure 11. The obtained τ_w distribution for smooth (left) and R1 (right) surface condition for KP505.

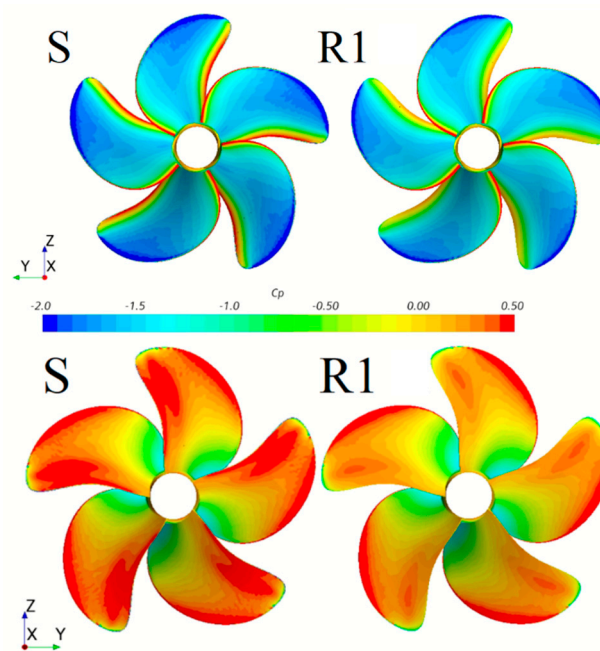


Figure 12. The obtained C_p distribution on KP505 surface for suction (**upper**) and pressure (**lower**) side of propeller.

5.3. The Impact of Hard Fouling on Propulsion Characteristics

After CFD simulations of resistance and open water tests are carried out, CFD simulations of SPT for smooth and fouled ships are performed. As said before, the fouling penalty on the ship performance should be considered through the change in P_D and n . The obtained increases in P_D and n due to the presence of hard fouling are presented in Figure 13. From this figure, it is clear that for surface conditions R1, R2 and R3 KVLCC2 is most affected due to the presence of hard fouling, while for surface conditions R4, R5 and R6 the fouling penalties for KVLCC2 and BC are almost the same and higher than fouling penalties for KCS. The obtained increases in P_D due to the presence of hard fouling for KVLCC2 range from 90.7% (R6) to 213.4% (R1), for BC range from 90.6% (R6) to 201.9% (R1) and for KCS range from 75.0% (R6) to 163.2% (R1), while the obtained increases in n for KVLCC2 range from 16.7% (R6) to 32.6% (R1), for BC range from 16.6% (R6) to 30.7% (R1) and for KCS range from 9.4% (R6) to 18.2% (R1). It is clear that the obtained increases in P_D are significantly higher than the obtained increases in P_E due to the presence of hard fouling, which can be related with the decrease in η_D . This highlights the importance of the assessment of the impact of biofouling on P_D rather than on P_E . The increase in P_D due to the presence of biofouling is dependent on many parameters. Thus, besides the portion of R_V in R_T , k/L and ship speed, which are important for the increase in P_E , it is also important at which J propeller operates and the way the propeller loading defined with K_T/J^2 is affected due to the presence of hard fouling. Namely, due to change in propeller loading, J value at which propeller operates changes as well. Thus, the change in J at which propeller operates as well as the absolute value of J is important, as, for ships which operate at higher J values, the fouling penalty on the propeller performance is higher.

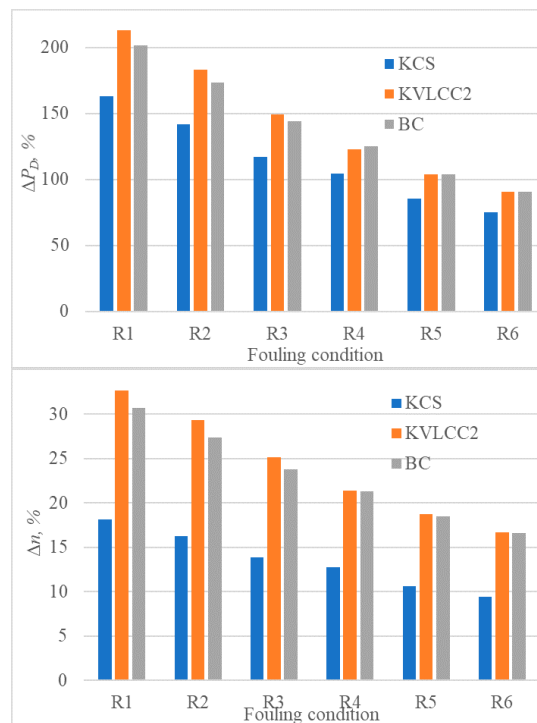


Figure 13. The obtained increases in P_D (upper) and η_H (lower) due to the presence of hard fouling.

In order to study the differences in the obtained fouling penalties more details, the impact of hard fouling on propulsion characteristics should be investigated. Within Tables 14–16, the obtained impact of hard fouling on propulsion characteristics is presented. From the obtained results, it is clear that most of the propulsion characteristics are affected by the presence of hard fouling on the hull and propeller surfaces. However, from Tables 14–16, it is clear that the impact of hard fouling on η_R is minimal, i.e., it is lower than 0.45% for all analyzed fouling conditions and ships. What is more, the impact of hard fouling on $1 - t$ is present, however, it is relatively low. Thus, due to the presence of hard fouling, the $1 - t$ value for KCS and KVLCC2 decreases, while for BC, it increases. It should be noted that the $1 - t$ value depends on many different parameters, i.e., on the fouling penalty related to increase in R_T , to propeller performance, as well as hull and propeller interaction. Obviously, the assessment of the effect of biofouling on $1 - t$ value is very complex. It should be noted that the obtained impact of hard fouling on $1 - t$ is within the obtained numerical uncertainty in the assessment of R_T and T . Additionally, within the assessment of $1 - t$, a modelling error is present as well, and it is related to turbulence modelling, modelling of the effect of ship propeller with body force method etc. Consequently, in order to assess this impact more accurately, numerical uncertainty as well as modelling error should be reduced through the application of more dense grids and lower time steps, as well as through the discretization of the propeller itself. Thus, a more accurate prediction of the impact of biofouling on $1 - t$ would be assessed. Therefore, based on the obtained results, it can be concluded that the impact of hard fouling on $1 - t$ is present, however, it is minimal. On the other hand, the impact of hard fouling on $1 - w$ is significant and detrimental, since it causes a decrease in the $1 - w$ value. Due to the presence of hard fouling, the obtained decreases in $1 - w$ values range from -6.99% (R6) to -11.7% (R1) for KCS, from -6.29% (R6) to -10.1% (R1) for KVLCC2 and from -8.46% (R6) to -12.0% (R1) for BC. The decrease in $1 - w$ can be attributed to slower flow around the propeller location for fouled ship, due to thicker boundary layer. The decrease in $1 - w$ has beneficial effect on η_H (Equation (11)). Thus, due to the presence of hard fouling the obtained $\Delta \eta_H$ values range from 6.13% (R6) to 11.3% (R1) for KCS, from 6.11% (R6) to 10.2% (R1) for KVLCC2 and from -11.3% (R6) to 16.9% (R1) for BC. Regardless of the fact that the decrease in $1 - w$ has beneficial effect on η_H , in general, the decrease in $1 - w$ has detrimental effect on η_D and P_D . Namely, the decrease in $1 - w$ points out

that the flow around propeller is slower and consequently propeller operating point is changed when compared with the smooth hull surface. Additionally, due to the presence of hard fouling, the nominal wake field behind the fouled ship is more inhomogeneous than nominal wake field behind the smooth ship, and because of this, the operating point is changed as well. Therefore, J for self-propulsion point decreases since v_A is lower. What is more, J for self-propulsion point decreases because of the increase in n as well. Due to the presence of hard fouling the obtained ΔJ values for self-propulsion point range from -15.0% (R6) to -25.3% (R1) for KCS, from -19.7% (R6) to -32.2% (R1) for KVLCC2 and from -21.5% (R6) to -32.6% (R1) for BC. The decrease in the J value is unfavorable, as KP 505, KP 458 and WB operate at J lower than J , for which the η_O function has a maximum value, which is common for all marine propellers. Consequently, due to the decrease in J value, η_O value decreases as well. The decrease in η_O value is related to the detrimental impact of hard fouling on the propeller performance in open water conditions. Thus, the obtained decreases in η_O values are higher than the obtained increases in η_H values. Due to the presence of hard fouling the obtained $\Delta\eta_O$ values range from -19.2% (R6) to -32.9% (R1) for KCS, from -21.1% (R6) to -37.3% (R1) for KVLCC2 and from -24.9% (R6) to -39.2% (R1) for BC. The obtained decreases in η_B values are similar to the ones obtained for η_O values, as the impact of hard fouling on η_R value is negligible. The presence of hard fouling, therefore, has two detrimental effects on η_O , because of detrimental effect on the open water characteristics and on the propeller operating point. These two effects can be equally meaningful. The importance of the impact of hard fouling on the propeller operating point can be seen from the obtained impact of biofouling on K_T values. Even though the presence of hard fouling on the propeller surfaces causes the decrease in K_T , due to the impact of hard fouling on the propeller operating point, K_T increases as J for self-propulsion point of fouled ship is lower than J for self-propulsion point of smooth ship. The obtained ΔK_T values due to the presence of hard fouling range from 26.8% (R6) to 42.6% (R1) for KCS, from 18.2% (R6) to 24.2% (R1) for KVLCC2 and from 15.1% (R6) to 22.1% (R1) for BC. The presence of hard fouling on hull and propeller surfaces causes an increase in K_Q due to two reasons. Firstly, due to the presence of hard fouling on propeller surfaces K_Q values in open water conditions are higher, and secondly due to the change in J for self-propulsion point K_Q value increases. The obtained increases in K_Q values due to the presence of hard fouling range from 33.6% (R6) to 59.6% (R1) for KCS, from 20.0% (R6) to 34.4% (R1) for KVLCC2 and from 20.2% (R6) to 35.3% (R1) for BC. Finally, from Tables 14–16, it is clear that the presence of hard fouling on the hull and propeller surfaces causes a significant decrease in η_D , since decreases in η_B are higher than increases in η_H . The obtained decreases in η_D values due to the presence of hard fouling range from -14.4% (R6) to -25.6% (R1) for KCS, from -16.1% (R6) to -31.0% (R1) for KVLCC2 and from -16.3% (R6) to -28.9% (R1) for BC. Since the impact of biofouling on η_D value is not negligible, the increases in P_E and P_D are not the same, and it is therefore necessary to investigate the impact of biofouling on P_D rather than on P_E . It should be noted that the results presented in this subsection are obtained for the presence of biofouling on both propeller and hull surfaces. For clean propeller surfaces and fouled ship hull the obtained results, i.e., trends may not be the same. Thus, Song et al. [22], have obtained slight increases in η_D values due to the presence of barnacles at hull surfaces, i.e., with a clean propeller. This can be attributed to the fact that the authors have obtained higher increases in η_H due to the presence of barnacles than decreases in η_B due to change in operating point. As a result of all this, the analysis of the impact of biofouling on propulsion characteristics is very important, i.e., the assessment of biofouling on the resistance characteristics and P_E is not sufficient.

Table 14. The obtained impact of hard fouling on the propulsion characteristics for KCS.

Propulsion Characteristic	S	R1	R2	R3	R4	R5	R6
$1 - t$	0.867	0.852 -1.67%	0.857 -1.15%	0.858 -1.07%	0.858 -1.06%	0.856 -1.28%	0.856 -1.29%
$1 - w$	0.773	0.682 -11.7%	0.690 -10.8%	0.699 -9.56%	0.707 -8.54%	0.714 -7.64%	0.719 -6.99%
η_H	1.122	1.249 11.3%	1.243 10.8%	1.227 9.39%	1.214 8.19%	1.199 6.89%	1.191 6.13%
η_O	0.700	0.470 -32.9%	0.489 -30.2%	0.514 -26.6%	0.527 -24.8%	0.553 -21.1%	0.566 -19.2%
η_R	1.002	0.998 -0.40%	1.000 -0.16%	0.999 -0.29%	1.000 -0.18%	1.001 -0.11%	1.000 -0.16%
η_D	0.787	0.585 -25.6%	0.607 -22.8%	0.630 -19.9%	0.639 -18.8%	0.663 -15.7%	0.674 -14.4%
J	0.729	0.545 -25.3%	0.560 -23.3%	0.579 -20.6%	0.592 -18.9%	0.609 -16.5%	0.620 -15.0%
K_T	0.165	0.236 42.6%	0.231 39.6%	0.224 35.6%	0.218 32.0%	0.214 29.3%	0.210 26.8%
$10K_Q$	0.274	0.436 59.6%	0.420 53.7%	0.402 47.0%	0.390 42.7%	0.374 36.9%	0.365 33.6%

Table 15. The obtained impact of hard fouling on the propulsion characteristics for KVLCC2.

Propulsion Characteristic	S	R1	R2	R3	R4	R5	R6
$1 - t$	0.820	0.812 -1.00%	0.812 -0.91%	0.813 -0.88%	0.813 -0.79%	0.814 -0.66%	0.815 -0.56%
$1 - w$	0.668	0.600 -10.1%	0.608 -9.02%	0.613 -8.19%	0.616 -7.75%	0.620 -7.17%	0.626 -6.29%
η_H	1.227	1.352 10.2%	1.337 8.91%	1.325 7.96%	1.320 7.55%	1.313 7.01%	1.302 6.11%
η_O	0.600	0.377 -37.3%	0.397 -34.0%	0.421 -29.9	0.448 -25.4%	0.461 -23.3%	0.474 -21.1%
η_R	0.998	0.997 -0.10%	1.002 0.35%	0.998 -0.02%	0.998 -0.02%	1.003 0.44%	1.001 0.28%
η_D	0.736	0.508 -31.0%	0.531 -27.8%	0.557 -24.4%	0.590 -19.8%	0.607 -17.6%	0.618 -16.1%
J	0.457	0.310 -32.2%	0.322 -29.7%	0.336 -26.6%	0.348 -24.0%	0.357 -21.8%	0.367 -19.7%
K_T	0.149	0.185 24.2%	0.183 23.4%	0.181 21.7%	0.182 22.4%	0.178 20.1%	0.176 18.2%
$10K_Q$	0.180	0.242 34.4%	0.236 31.0%	0.230 27.4%	0.225 24.7%	0.220 21.8%	0.216 20.0%

From the results presented in Tables 14–16, it can be concluded that the impact of hard fouling on the propulsion characteristics is the most pronounced for BC. Namely, the obtained changes in $1 - t$, $1 - w$, J , η_H , η_O and η_B due to the presence of hard fouling are largest for BC. What is more, the obtained changes in η_D due to the presence of hard fouling for fouling conditions R4, R5 and R6 are the largest for BC as well. However, for fouling conditions R1, R2 and R3 the obtained decreases in η_D are larger for KVLCC2 than for BC. For these fouling conditions, larger increase in η_H which is obtained for BC has surpassed the larger decrease in η_B , which has also been obtained for BC and because of this the obtained decreases in η_D are larger for KVLCC2. The largest changes in ΔK_T and ΔK_Q are obtained for KCS and this can be attributed to the fact that KCS operates at a higher J value than KVLCC2 and BC. The largest decrease in the ratio between K_T and K_Q has been noticed, due to the presence of hard fouling for KCS as well. Nevertheless, amongst the investigated ships, the decrease in η_O is the lowest, which can be attributed through the lowest obtained decrease in J for KCS. Namely, J for self-propulsion point decreases due to the increases in n and $1 - w$. As can be seen from Figure 13,

the obtained increases in n due to the presence of hard fouling are significantly lower for KCS than for KVLCC2 and BC, while increases in $1 - w$ due to the presence of hard fouling are relatively similar for all analyzed ships, Tables 14–16.

Table 16. The obtained impact of hard fouling on the propulsion characteristics for BC.

Propulsion Characteristic	S	R1	R2	R3	R4	R5	R6
$1 - t$	0.764	0.787 2.95%	0.785 2.76%	0.782 2.31%	0.781 2.22%	0.779 1.95%	0.779 1.88%
$1 - w$	0.653	0.575 -12.0%	0.579 -11.3%	0.583 -10.7%	0.590 -9.68%	0.595 -8.89%	0.598 -8.46%
η_H	1.171	1.369 16.9%	1.356 15.8%	1.341 14.5%	1.325 13.2%	1.310 11.9%	1.303 11.3%
η_O	0.622	0.378 -39.2%	0.396 -36.4%	0.416 -33.1%	0.436 -30.0%	0.456 -26.8%	0.468 -24.9%
η_R	1.000	1.000 -0.03%	0.999 -0.09%	1.001 0.10%	0.999 -0.14%	0.999 -0.15%	1.001 0.10%
η_D	0.729	0.518 -28.9%	0.536 -26.4%	0.559 -23.4%	0.577 -20.8%	0.596 -18.2%	0.61 -16.3%
J	0.533	0.359 -32.6%	0.371 -30.3%	0.384 -27.8%	0.397 -25.6%	0.410 -23.1%	0.418 -21.5%
K_T	0.183	0.224 22.1%	0.221 20.8%	0.219 19.3%	0.217 18.4%	0.213 16.4%	0.211 15.1%
$10K_Q$	0.250	0.338 35.3%	0.331 32.5%	0.321 28.6%	0.314 26.0%	0.306 22.5%	0.300 20.2%

5.4. The Impact of Hard Fouling on the Flow Around Fouled Ship

The impact of hard fouling on the ship performance is investigated for three ships at their design speeds presented in Table 2. This resulted in different τ_w distributions for smooth surface condition, Figure 14. From this figure it is clear that the highest τ_w values are obtained for KCS, followed by BC and KVLCC2, which was expected as KCS is investigated at the highest design speed. As a result of this, the highest k^+ values are also obtained along the KCS hull, which can be seen from Figure 15. The obtained k^+ distributions for R1 fouling condition along the KCS, KVLCC2 and BC hull are shown. Since the highest k^+ values are obtained along the KCS hull, the highest ΔU^+ values are present as well, which resulted in more significant increase in τ_w and C_F for KCS than for BC and KVLCC2. The obtained τ_w distributions for R1 fouling condition along the KCS, KVLCC2 and BC hull are presented in Figure 16.

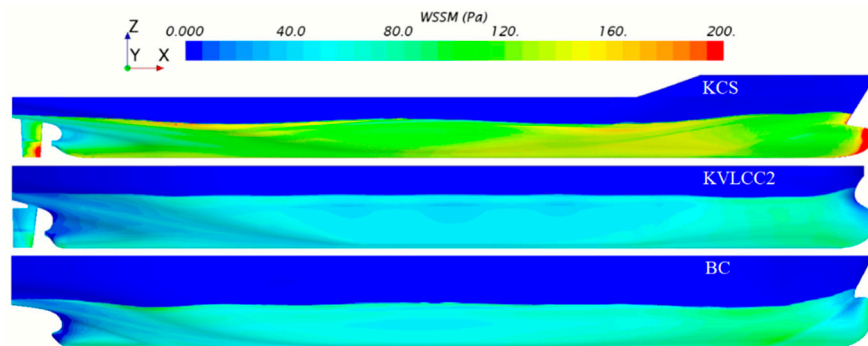


Figure 14. The obtained τ_w distributions for smooth surface condition along the KCS (upper), KVLCC2 (middle) and BC (lower) hull.

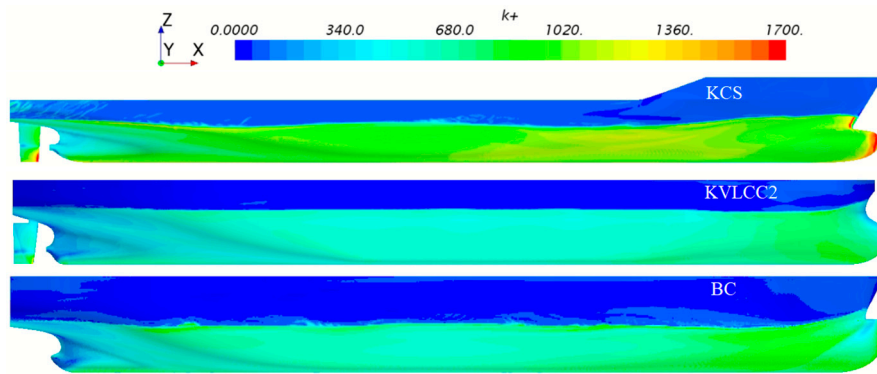


Figure 15. The obtained k^+ distributions for R1 fouling condition along the KCS (upper), KVLCC2 (middle) and BC (lower) hull.

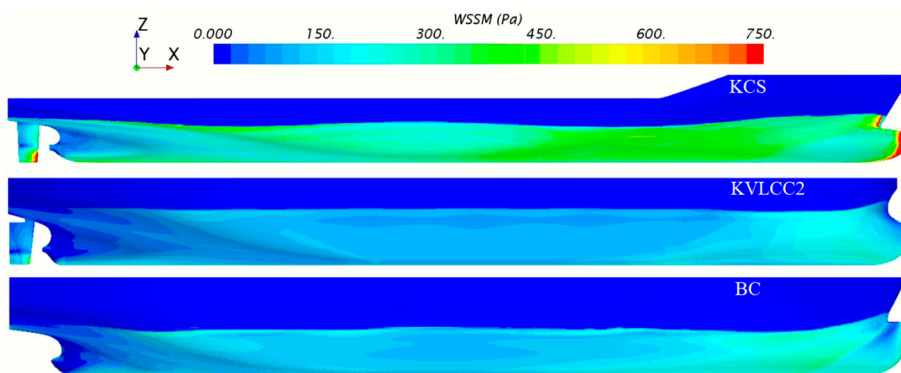


Figure 16. The obtained τ_w distributions for R1 fouling condition along the KCS (upper), KVLCC2 (middle) and BC (lower) hull.

The increase in τ_w along the hull causes a decrease in the velocity in the turbulent boundary layer, i.e., turbulent boundary layer thickness increases due to the presence of roughness, which can be seen from Figure 17. In this figure, boundary layers, which are defined as the distance between the hull surface and the point where the axial velocity magnitude of the flow reaches the proportion of 0.99 of the ship speed, are shown for smooth and R1 surface condition. The boundary layers for KCS are given at locations $x = 30$ m and $x = 50$ m, for KVLCC2 at locations $x = 50$ m and $x = 70$ m and for BC at $x = 17.5$ m and $x = 35$ m. The obtained increases in the boundary layer thickness, due to the presence of biofouling or roughness, is in line with previously published experimental results in the literature [43,44].

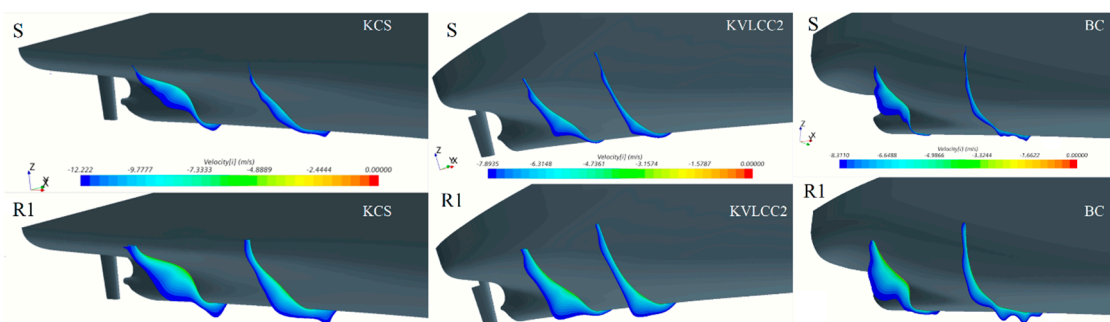


Figure 17. The obtained boundary layers for smooth ships (upper) and fouled ships with fouling condition R1 (lower).

As the boundary layer thickness increases it is obvious that the presence of hard fouling will cause the change in the nominal wake distribution. In Figure 18, the obtained contours of $1 - w_N$ for

smooth and fouled ships (R1) in the propeller disc plane are shown. It should be noted that $1 - w_N$ is calculated as the ratio between axial velocity and ship speed [45]. From this figure, it is clear that the presence of hard fouling causes the significant reduction of the flow in the propeller disc plane for all three investigated ships. This reduction causes the change of J for self-propulsion point and in that way, it affects propeller efficiency, as already explained.

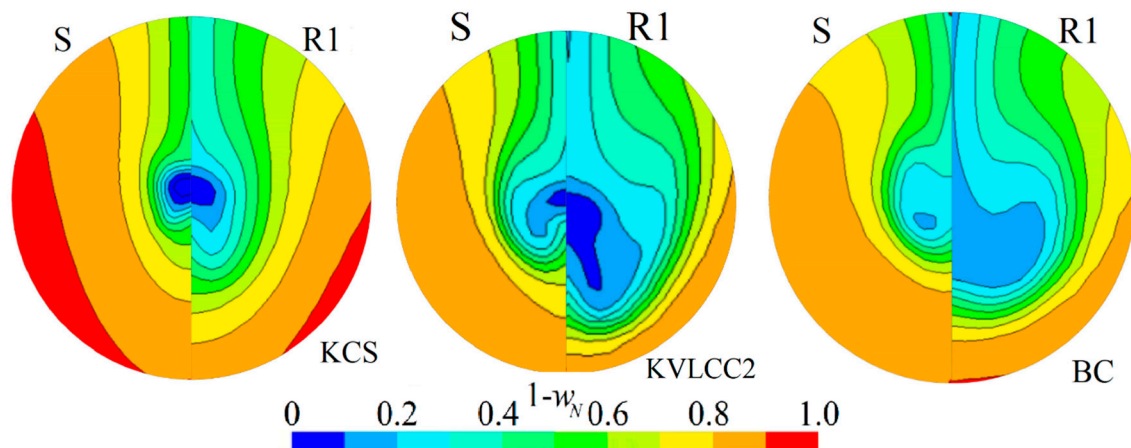


Figure 18. The obtained contours of $1 - w_N$ for smooth and fouled KCS (left), KVLCC2 (middle) and BC (right) with fouling condition R1 in the propeller disc plane.

In addition to the impact of hard fouling on τ_w values, the presence of hard fouling causes the change in pressure distribution along the hull. However, this change mainly occurs in the area near the stern of fouled ship [16]. In Figure 19, the obtained C_p distributions are presented for the area near the stern of investigated ships for smooth and R1 fouling conditions within CFD simulations of SPT. It should be noted that C_p is obtained as a ratio between pressure and $\frac{1}{2}\rho v^2$. From this figure, it is clear that due to the presence of hard fouling pressure recovery at the stern is reduced and because of this R_{VP} increases. Additionally, the impact of hull and propeller fouling on C_p distribution at the rudder can be noticed, i.e., C_p values at the rudder surface are slightly reduced.

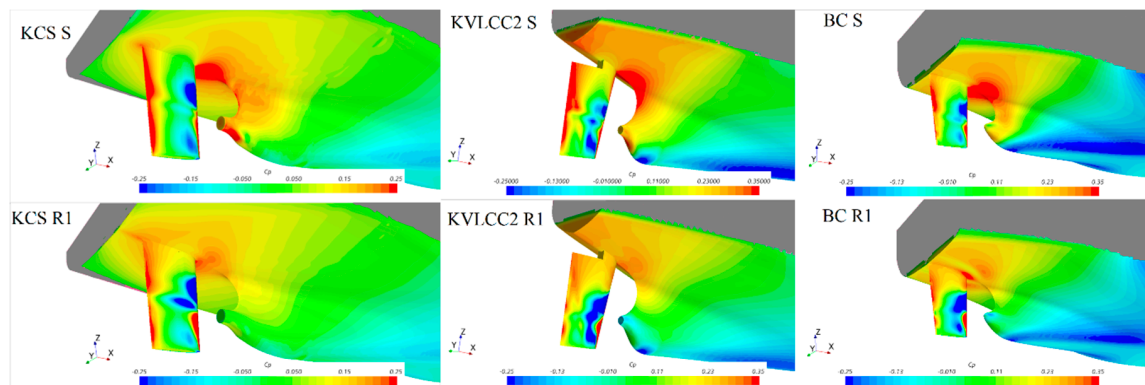


Figure 19. The impact of hard fouling on C_p distribution for the area near the stern.

In Figure 20, the obtained wave patterns around the hulls of the investigated ships for smooth surface condition and R1 fouling condition from CFD simulations of resistance tests are presented. From the comparison between wave pattern for smooth KCS and BC and wave pattern for KCS and BC fouled with R1, it can be noticed that due the presence of hard fouling wave elevations are reduced. On the other hand, wave elevations for KVLCC2 are almost the same for smooth and R1 fouling condition. The similar finding is noticed within [16,20]. Reductions of wave elevations and consequently R_W , due to the presence of hard fouling can be related to the increase in viscosity [15].

It can be concluded that the impact of hard fouling on the wave elevations is in agreement with the obtained decreases in R_W , i.e., for KCS and BC this impact is relevant, while for KVLCC2 this impact is negligible.

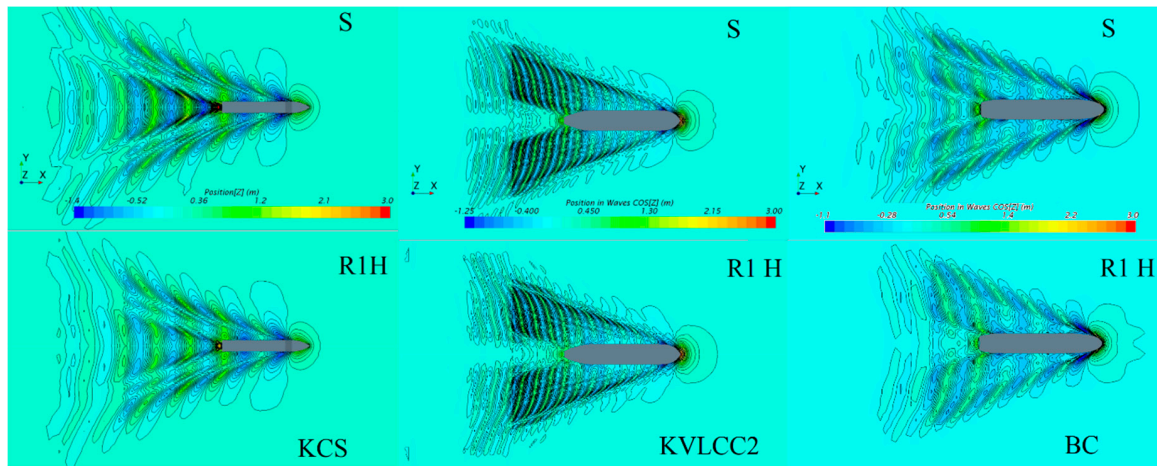


Figure 20. The obtained wave patterns around KCS (left), KVLCC2 (middle) and BC (right).

6. Conclusions

In this paper, the impact of hard fouling on ship performance for three different ship types is investigated. This impact is investigated using the CFD simulations of resistance, open water and self-propulsion tests. The impact of hard fouling is represented through the modification of wall function, i.e., through the implementation of the Grigson ΔU^+ model in the wall function within CFD solver. The verification study for grid size and time step is carried out, and grid and temporal uncertainties are estimated using GCI method. The verification study is performed for several key variables, i.e., K_{TO} and K_{QO} for open water test and for P_D , n , T and J for self-propulsion test. Relatively low simulation uncertainties are obtained for all key variables. Thereafter, the obtained results of the performed CFD simulations for smooth surface condition are validated with the extrapolated towing tank results using the ITTC 1978 Performance Prediction Method. Satisfactory agreement is achieved for all resistance, open water and propulsion characteristics. After the verification and validation study, the impact of hard fouling on the ship performance is studied in terms of the impact on resistance, open water and propulsion characteristics. The obtained results demonstrated the significant impact of hard fouling on the increase in frictional resistance and viscous resistance, as well for all three ships. It should be noted that the viscous resistance of KCS is mostly affected due to the presence of hard fouling, which is ascribed to the fact that KCS is investigated at the highest speed. As a result of this, friction velocity along the KCS hull is higher than along the KVLCC2 and BC hulls. Higher ΔU^+ values are obtained along the KCS hull in comparison with KVLCC2 and BC hulls, since the roughness Reynolds number and therefore ΔU^+ are dependent on the friction velocity. However, wave resistance has decreased for KCS and BC, due to the presence of hard fouling, while for KVLCC2, it is almost negligible, and has remained almost the same as for smooth surface condition. The impact of hard fouling on the wave resistance is in agreement with the impact of hard fouling on the wave elevations, i.e., wave elevations for KCS and BC due to the presence of hard fouling are decreased, while for KVLCC2, it remained the same as for the smooth surface condition. Therefore, the most affected ship due to the presence of hard fouling, related to the fouling penalty on the ship resistance, is KVLCC2. Obviously, beside the ship speed the portion of viscous resistance in total resistance is very important for the estimation of the fouling penalty on the ship resistance, as well as the ratio k/L . Significant detrimental effects due to the presence of hard fouling on the propeller performance in open water conditions are found. Thus, due to the presence of hard fouling on the propeller surfaces, K_{TO} decreases and K_{QO} increases, which results in a significant decrease in η_O . Namely, due to the

presence of hard fouling drag coefficient of propeller blade section increases, causing the increase in K_{QO} , and lift coefficient decreases, causing the decrease in K_{TO} . The impact of hard fouling on the ship performance is best reflected through the impact on the delivered power and propeller rotation rate. From the obtained results, it is clear that increases in the delivered power are significantly larger than increases in the effective power, due to the presence of hard fouling for all three investigated ships. Therefore, the impact of hard fouling on propulsion efficiency must not be neglected, especially for fouled ship and propeller. The impact of hard fouling on the delivered power and propeller rotation rate is most pronounced for KVLCC2 for fouling conditions R1, R2 and R3, while for R4, R5 and R6, the obtained changes in the ship performance due to hard fouling are similar for BC and KVLCC2. This can be attributed to different impact of hard fouling on propulsion characteristics, as the fouling penalty on effective power for R4, R5 and R6 fouling conditions is higher for KVLCC2 than for BC. Namely, the additional important parameter that affects the impact of biofouling on the ship performance is the value of advance coefficient for self-propulsion point, since it is demonstrated that ships which operate at higher values of advance coefficient will be more affected in terms of propeller performance in open water conditions than ships which operate at lower values of advance coefficient. The impact of hard fouling on propulsion characteristics is presented for all three ships. From the obtained results it can be seen that propulsion characteristics of BC are mostly affected due to the presence of hard fouling, as the obtained changes in $1 - t$, $1 - w$, J , η_H , η_O and η_B due to the presence of hard fouling are largest for BC. Additionally, the obtained changes in η_D due to the presence of hard fouling for fouling conditions R4, R5 and R6 are the largest for BC as well, while, for R1, R2 and R3, they are the largest for KVLCC2. The largest change in K_T and K_Q values due to the presence of hard fouling are obtained for KCS, which is expected as KCS operate with the highest advance coefficient. Finally, the impact of hard fouling on the flow around fouled ship is studied through the analysis of the impact on wall shear stress distribution, boundary layer thickness, nominal wake distributions, wave elevations and pressure distributions.

The paper provided several valuable insights related to the impact of hard fouling on the ship performance amongst different ship forms. Future study will be focused on investigations related to the impact of biofouling for systematic series of certain ship at different speeds, which will allow more comprehensive insight into the impact of biofouling on the ship performance will be assessed. In this paper, the investigations related to the impact of hard fouling on the ship performance are performed for the presence of hard fouling on both propeller and hull surfaces. If analyzed per unit area, the impact of propeller fouling condition on the ship performance is significantly more important than the impact of hull fouling condition. Therefore, the future studies will be also focused on the investigations related to the impact of solely propeller cleaning on the ship performance. Thus, relatively cheap and effective practice for achieving significant energy saving will be demonstrated. The optimization of maintenance schedule is an important operational measure for reducing ship emissions and the successful application of this measure relies on the accurate assessment of the impact of cleaning, i.e., the impact of biofouling on the ship performance. Currently, these predictions are carried out using performance monitoring. However, performance monitoring has several important drawbacks [8], and the approach presented in this paper presents another way for this assessment. The important benefit of the proposed approach over the performance monitoring is that fouling effects on the ship performance can be analyzed independently of all other additional resistances, which may occur during sailing. However, since drag characterization studies are performed only for limited number of fouling conditions, CFD approach based on the modified wall function approach is limited to these fouling conditions. For more comprehensive assessment there is a need for further drag characterization studies. Additionally, the investigations performed in this paper are carried out for hull surface, which is treated as a uniformly rough surface with certain roughness length scale determined using Equation (6), as done in most of the conventional CFD studies dealing with biofouling. Since the fouling pattern along the immersed surface is not uniform, future studies will be focused on the investigations of the influence of fouling settlement on the ship performance. The locations of niche

areas along the hull surface will be found from the literature and in that areas, wall function model for certain fouling condition will be implemented within the wall function of CFD solver. In that way, more realistic fouling conditions will be analyzed, and the investigations regarding the partial cleaning of the ship hull will be performed as well. Based on that, the proposed method can be used for the assessment of fouling penalties on the ship performance, after the fouling condition of the hull and propeller are determined by divers in the port.

Author Contributions: Conceptualization, A.F. and N.D.; methodology, A.F., N.D., I.M. and R.D.; software, A.F.; validation, A.F.; formal analysis, A.F.; investigation, A.F., N.D. and I.M.; resources, A.F.; writing—Original draft preparation, A.F., N.D., I.M. and R.D.; writing—Review and editing, A.F., N.D., I.M. and R.D.; visualization, A.F.; supervision, N.D. All authors have read and agreed to the published version of the manuscript.

Funding: This research received no external funding.

Conflicts of Interest: The authors declare no conflict of interest.

Abbreviations

AF	antifouling
CFD	Computational Fluid Dynamics
GCI	Grid Convergence Index
GHG	Greenhouse Gas
ITTC	International Towing Tank Conference
MRF	Moving Reference Frame
PPM	Performance Prediction Method
OWT	Open Water Test
RANS	Reynolds Averaged Navier-Stokes
RD	Relative Deviation
R1-R6	fouling conditions
S	Smooth surface condition
SPT	Self-Propulsion Test
VOF	Volume Of Fluid
HRIC	High Resolution Interface Capturing
FVM	Finite Volume Method
SST	Shear Stress Transport
KCS	Kriso Container Ship
KVLCC2	Kriso Very Large Crude Carrier 2
BC	Bulk Carrier
B	breadth (m)
B	smooth wall log-law intercept (-)
C_B	block coefficient (-)
C_F	frictional resistance coefficient (-)
C_P	pressure coefficient (-)
C_T	total resistance coefficient (-)
C_W	wave resistance coefficient (-)
c	chord length at radius $0.75R$ (m)
D	propeller diameter (m)
d	shaft diameter (m)
Fn	Froude number (-)
J	advance coefficient (-)
k	roughness length scale (μm)
k	form factor (-)
k^+	roughness Reynolds number (-)
K_T	thrust coefficient (-)
K_Q	torque coefficient (-)
K_{TO}	thrust coefficient in open water conditions (-)

K_{QO}	torque coefficient in open water conditions (-)
L_{pp}	length between perpendiculars (m)
L_{wl}	length of waterline (m)
n	propeller rate of revolution (rpm)
S	wetted surface area (m ²)
P	propeller pitch (m)
\bar{p}	mean pressure (Pa)
P_E	effective power (W)
P_D	delivered power at propeller (W)
Rn	Reynolds number (-)
R	propeller radius (m)
R_F	frictional resistance (N)
R_T	total resistance (N)
R_t	height of the largest barnacle (μm)
R_V	viscous resistance (N)
R_{VP}	viscous pressure resistance (N)
T	thrust (N)
T	time interval calculated as the ratio between ship length and speed (s)
T	draught (m)
t	thrust deduction fraction (-)
t	maximum thickness at radius $0.75R$ (mm)
\bar{u}_i	averaged velocity vector (m/s)
U^+	non-dimensional mean velocity (-)
U_G	grid uncertainty (-)
U_J	numerical uncertainty in the prediction of J (-)
U_n	numerical uncertainty in the prediction of n (-)
U_{P_D}	numerical uncertainty in the prediction of P_D (-)
U_T	time step uncertainty (-)
U_T	numerical uncertainty in the prediction of T (-)
u_τ	friction velocity (m/s)
v	speed (m/s)
V	ship design speed (kn)
y^+	non-dimensional wall distance (-)
w	wake fraction coefficient (-)
Z	number of blades (-)
%SC	percentage of the surface coverage (-)
Δ	displacement (t)
ΔU^+	roughness function (-)
$\Delta\phi$	change in certain hydrodynamic characteristic (-)
∇	displacement volume (m ³)
η_B	propeller efficiency behind ship (-)
η_D	quasi-propulsive efficiency coefficient (-)
η_H	hull efficiency (-)
η_O	propeller efficiency in open water (-)
η_R	relative rotative efficiency (-)
κ	von Karman constant (-)
μ	dynamic viscosity coefficient (Pas)
ρ	fluid density (kg/m ³)
$\overline{\rho u'_i u'_j}$	Reynolds stress tensor (N/m ²)
$\bar{\tau}_{ij}$	mean viscous stress tensor (N/m ²)
τ_w	wall shear stress (N/m ²)
ϕ	certain hydrodynamic characteristic (-)
ϕ_{ext}^{21}	extrapolated value (-)
EXP	experimental

EX	extrapolated
M	ship model
R	fouled surface
S	smooth surface
1	fine grid/time step
2	medium grid/time step
3	coarse grid/time step

References

- Bouman, E.A.; Lindstad, E.; Rialland, A.I.; Stromman, A.H. State-of-the-art technologies, measures, and potential for reducing GHG emissions from shipping—A review. *Transp. Res. D Transp. Environ.* **2017**, *52*, 408–421. [[CrossRef](#)]
- Corbett, J.J.; Wang, H.; Winebrake, J.J. The effectiveness and costs of speed reductions on emissions from international shipping. *Transp. Res. D Transp. Environ.* **2009**, *14*, 593–598. [[CrossRef](#)]
- Poulsen, R.T.; Johnson, H. The logic of business vs. the logic of energy management practice: Understanding the choices and effects of energy consumption monitoring systems in shipping companies. *J. Clean. Prod.* **2016**, *112*, 3785–3797. [[CrossRef](#)]
- Adland, R.; Cariou, P.; Jia, H.; Wolff, F.C. The energy efficiency effects of periodic ship hull cleaning. *J. Clean. Prod.* **2018**, *178*, 1–13. [[CrossRef](#)]
- Farkas, A.; Degiuli, N.; Martić, I. Towards the prediction of the effect of biofilm on the ship resistance using CFD. *Ocean Eng.* **2018**, *167*, 169–186. [[CrossRef](#)]
- Schultz, M.P.; Bendick, J.A.; Holm, E.R.; Hertel, W.M. Economic impact of biofouling on a naval surface ship. *Biofouling* **2011**, *27*, 87–98. [[CrossRef](#)] [[PubMed](#)]
- Uzun, D.; Demirel, Y.K.; Coraddu, A.; Turan, O. Time-dependent biofouling growth model for predicting the effects of biofouling on ship resistance and powering. *Ocean Eng.* **2019**, *191*, 106432. [[CrossRef](#)]
- Farkas, A.; Song, S.; Degiuli, N.; Martić, I.; Demirel, Y.K. Impact of biofilm on the ship propulsion characteristics and the speed reduction. *Ocean Eng.* **2020**, *199*, 107033. [[CrossRef](#)]
- Yeginbayeva, I.A.; Granhag, L.; Chernoray, V. Review and historical overview of experimental facilities used in hull coating hydrodynamic tests. *Proc. Inst. Mech. Eng. Part M J. Eng. Marit. Environ.* **2019**, *233*, 1240–1259. [[CrossRef](#)]
- Uzun, D.; Ozyurt, R.; Demirel, Y.K.; Turan, O. Does the barnacle settlement pattern affect ship resistance and powering? *Appl. Ocean Res.* **2020**, *95*, 102020. [[CrossRef](#)]
- Demirel, Y.K.; Uzun, D.; Zhang, Y.; Fang, H.C.; Day, A.H.; Turan, O. Effect of barnacle fouling on ship resistance and powering. *Biofouling* **2017**, *33*, 819–834. [[CrossRef](#)] [[PubMed](#)]
- Schultz, M.P. Frictional resistance of antifouling coating systems. *J. Fluids Eng.* **2004**, *126*, 1039–1047. [[CrossRef](#)]
- Demirel, Y.K.; Song, S.; Turan, O.; Incecik, A. Practical added resistance diagrams to predict fouling impact on ship performance. *Ocean Eng.* **2019**, *186*, 106112. [[CrossRef](#)]
- Schultz, M.P. Effects of coating roughness and biofouling on ship resistance and powering. *Biofouling* **2007**, *23*, 331–341. [[CrossRef](#)]
- Demirel, Y.K.; Turan, O.; Incecik, A. Predicting the effect of biofouling on ship resistance using CFD. *Appl. Ocean Res.* **2017**, *62*, 100–118. [[CrossRef](#)]
- Farkas, A.; Degiuli, N.; Martić, I. An investigation into the effect of hard fouling on the ship resistance using CFD. *Appl. Ocean Res.* **2020**, *100*, 102205. [[CrossRef](#)]
- Song, S.; Demirel, Y.K.; Atlar, M. An investigation into the effect of biofouling on the ship hydrodynamic characteristics using CFD. *Ocean Eng.* **2019**, *175*, 122–137. [[CrossRef](#)]
- Farkas, A.; Degiuli, N.; Martić, I. Impact of biofilm on the resistance characteristics and nominal wake. *Proc. Inst. Mech. Eng. Part M J. Eng. Marit. Environ.* **2020**, *234*, 59–75. [[CrossRef](#)]
- Andersson, J.; Oliveira, D.R.; Yeginbayeva, I.; Leer-Andersen, M.; Bensow, R.E. Review and comparison of methods to model ship hull roughness. *Appl. Ocean Res.* **2020**, *99*, 102119. [[CrossRef](#)]
- Song, S.; Demirel, Y.K.; Muscat-Fenech, C.D.M.; Tezdogan, T.; Atlar, M. Fouling effect on the resistance of different ship types. *Ocean Eng.* **2020**, *216*, 107736. [[CrossRef](#)]

21. Song, S.; Demirel, Y.K.; Atlar, M.; Dai, S.; Day, S.; Turan, O. Validation of the CFD approach for modelling roughness effect on ship resistance. *Ocean Eng.* **2020**, *200*, 107029. [CrossRef]
22. Song, S.; Demirel, Y.K.; Atlar, M. Penalty of hull and propeller fouling on ship self-propulsion performance. *Appl. Ocean Res.* **2020**, *94*, 102006. [CrossRef]
23. Leer-Andersen, M.; Larsson, L. An Experimental/Numerical Approach for Evaluating Skin Friction on Full-Scale Ships with Surface Roughness. *J. Mar. Sci. Technol.* **2003**, *8*, 26–36. [CrossRef]
24. Bradshaw, P. A Note on “Critical Roughness Height” and “Transitional Roughness”. *Phys. Fluids* **2000**, *12*, 1611–1614. [CrossRef]
25. Farkas, A.; Degiuli, N.; Martić, I. Assessment of hydrodynamic characteristics of a full-scale ship at different draughts. *Ocean Eng.* **2018**, *156*, 135–152. [CrossRef]
26. IMO. *Third IMO GHG Study 2014*; International Maritime Organization (IMO): London, UK, 2014.
27. Kim, W.J.; Van, S.H.; Kim, D.H. Measurement of flows around modern commercial ship models. *Exp. Fluids* **2001**, *31*, 567–578. [CrossRef]
28. Hino, T.; Kenkyujo, K.G.A. *Proceedings of CFD Workshop Tokyo 2005*; National Maritime Research Institute: Tokyo, Japan, 2005.
29. Brodarski Institute. *Report 6389-M. Technical Report*; Brodarski Institute: Zagreb, Croatia, 2014.
30. ITTC. Recommended procedures and guidelines. In *1978 ITTC Performance Prediction Method*; ITTC: Bournemouth, UK, 1999.
31. Larsson, L.; Stern, F.; Visonneau, M.; Hino, T.; Hirata, N.; Kim, J. *Proceedings, Tokyo 2015 Workshop on CFD in Ship Hydrodynamics*; NMRI: Tokyo, Japan, 2015.
32. SIMMAN. 2008. Available online: <http://www.simman2008.dk/> (accessed on 1 September 2020).
33. Farkas, A.; Degiuli, N.; Martić, I. Numerical investigation into the interaction of resistance components for a series 60 catamaran. *Ocean Eng.* **2017**, *146*, 151–169. [CrossRef]
34. Farkas, A.; Degiuli, N.; Martić, I.; Ančić, I. Performance prediction method for fouled surfaces. *Appl. Ocean Res.* **2020**, *99*, 102151. [CrossRef]
35. Tezdogan, T.; Demirel, Y.K.; Kellett, P.; Khorasanchi, M.; Incecik, A.; Turan, O. Full-scale unsteady RANS CFD simulations of ship behaviour and performance in head seas due to slow steaming. *Ocean Eng.* **2015**, *97*, 186–206. [CrossRef]
36. Terziev, M.; Tezdogan, T.; Incecik, A. Application of eddy-viscosity turbulence models to problems in ship hydrodynamics. *Ships Offshore Struct.* **2020**, *15*, 511–534. [CrossRef]
37. Terziev, M.; Tezdogan, T.; Oguz, E.; Gourlay, T.; Demirel, Y.K.; Incecik, A. Numerical investigation of the behaviour and performance of ships advancing through restricted shallow waters. *J. Fluid Struct.* **2018**, *76*, 185–215. [CrossRef]
38. Owen, D.; Demirel, Y.K.; Oguz, E.; Tezdogan, T.; Incecik, A. Investigating the effect of biofouling on propeller characteristics using CFD. *Ocean Eng.* **2018**, *159*, 505–516. [CrossRef]
39. Song, S.; Demirel, Y.K.; Atlar, M. Propeller performance penalty of biofouling: Computational fluid dynamics prediction. *J. Offshore Mech. Arct.* **2020**, *142*. [CrossRef]
40. Choi, J.E.; Min, K.S.; Kim, J.H.; Lee, S.B.; Seo, H.W. Resistance and propulsion characteristics of various commercial ships based on CFD results. *Ocean Eng.* **2010**, *37*, 549–566. [CrossRef]
41. Gaggero, S.; Villa, D.; Viviani, M. An extensive analysis of numerical ship self-propulsion prediction via a coupled BEM/RANS approach. *Appl. Ocean Res.* **2017**, *66*, 55–78. [CrossRef]
42. Castro, A.M.; Carrica, P.M.; Stern, F. Full scale self-propulsion computations using discretized propeller for the KRISO container ship KCS. *Comput. Fluids* **2011**, *51*, 35–47. [CrossRef]
43. Schultz, M.P.; Flack, K.A. The rough-wall turbulent boundary layer from the hydraulically smooth to the fully rough regime. *J. Fluid Mech.* **2007**, *580*, 381. [CrossRef]
44. Flack, K.A.; Schultz, M.P.; Connelly, J.S. Examination of a critical roughness height for outer layer similarity. *Phys. Fluids* **2007**, *19*, 095104. [CrossRef]
45. Farkas, A.; Degiuli, N.; Martić, I.; Dejhalla, R. Numerical and experimental assessment of nominal wake for a bulk carrier. *J. Mar. Sci. Technol.* **2019**, *24*, 1092–1104. [CrossRef]

